DUAL THERAPY OPPORTUNITIES FOR TUBERCULOSIS AND PROSTATE CANCER BASED ON CRYSTAL ENGINEERING PRINCIPLES

A Thesis Submitted to
the Graduate School of Engineering and Sciences of
İzmir Institute of Technology
in Partial Fulfillment of the Requirements for the Degree of

MASTER OF SCIENCE

in Biotechnology

by
Merve ARPACIOĞLU

December 2019
İZMİR

We approve the thesis of **Merve ARPACIOĞLU**

Examining Committee Members:

Prof. Dr. Gülşah ŞANLI MOHAMED
Department of Chemistry, İzmir Institute of Technology

Prof. Dr. Işıl SÖZÜER
Department of Chemistry, İzmir Institute of Technology

Prof. Dr. Şenay ŞANLIER
Department of Biochemistry, Ege University

19 December 2019

Prof. Dr. Gülşah ŞANLI MOHAMED
Supervisor,
Department of Chemistry
İzmir Institute of Technology

Prof. Dr. Gülşah ŞANLI MOHAMED
Head of the Department of Biotechnology

Prof. Dr. Mehtap EMİRDAĞ EANES
Dean of the Graduate School of
Engineering and Science

ACKNOWLEDGMENT

First of all, I would like to express my kindest thanks to Prof. Dr. Gülşah Şanlı Mohamed for the encouragement, the believe in me and invaluable assistance I have received. Additionally, I would like to thank Professor Teresa Duarte for being part of her research group, enlarging my vision and knowledge throughout my Erasmus+ mobility action at Instituto Superior Tecnico.

Second of all, I would like to express my gratitude and special thanks to my mentor, Dr. Vania André and Research Assistant Derya Mete Bostanbaş for their professional guidance, mentorship, dearest understanding, and countless help I have received, not only professionally but also with any problem occurred during my stay in both İzmir and Lisbon. This thesis could not have been made without their contributions.

Moreover, I would like to tell my special thanks for research members of Şanlı and Centro de Química Estrutural, whom were also there for me with their professional help anytime.

Asides from all, I am extremely thankful to Prof. Dr. Gülsah Sanli Mohammed, who supported me for my mobility action in the first place.

Yet, my deepest gratitude goes to my beloved family members, Ibrahim Arpacioglu, Sevim Arpacioglu and Metin Arpacioglu, for their endless support and believe in me, which I have had during my entire life.

Last but not least, I am grateful to my all friends from Turkey, particularly Gözde Yeşiltaş, and Eng. Domenico Bravo, for making my stay more delightful with his company and ever-lasting friendship in Lisbon.

ABSTRACT

DUAL THERAPY OPPORTUNITIES FOR TUBERCULOSIS AND PROSTATE CANCER BASED ON CRYSTAL ENGINEERING PRINCIPLES

Within this work, it is aimed to facilitate dual therapy opportunities for the treatment of tuberculosis and prostate cancer separately based on crystal engineering principles. In this regard, a quinolone family member antibiotic namely Sparfloxacin (SPX) is combined with another antibiotic called 4-aminosalicylic acid (4-ASA). Due to the drug-drug combination, it is expected to have superior biological activity since both drugs are stated and offered to be used in the treatment of tuberculosis. In addition to that, Apalutamide (APA) a recent drug in the treatment of castration-sensitive metastatic prostate cancer (CSMPC), is metallo-encapsulated by using zeolitic imidazolate framework-8 (ZIF-8). Owing to pH-sensitive decomposition, the new formulation is expected to combine the benefit of free zinc release and APA release to the targeted cancerous section. Both new compounds are synthesized characterized by various methods such as single crystal X-ray diffraction (SCXRD), powder X-ray diffraction (PXRD), Fourier-transform infrared radiation (FTIR), thermal gravimetric analysis (TGA), differential scanning calorimetry (DSC), scanning electron microscopy (SEM) and high-performance liquid chromatography (HPLC).

ÖZET

KRİSTAL MÜHENDİSLİĞİ PRENSİPLERİNE DAYALI TÜBERKÜLOZ VE PROSTAT KANSERİNDE KULLANILMAK ÜZERE ÇİFT YÖNLÜ TERAPİ SEÇENEKLERİ

Bu çalışmada, tüberküloz ve prostat kanserinin tedavisi için kristal mühendisliği prensiplerine dayalı ikili etkiye sahip terapi fırsatlarının kolaylaştırılması amaçlanmaktadır. Bu bağlamda, bir kinolon ailesi üyesi olan antibiyotik, yani Sparfloksasin (SPX), 4-aminosalisilik asit (4-ASA) antibiyotiği ile birleştirilecektir. İlaç-ilaç kombinasyonundan sayesinde, her iki ilacın tüberküloz tedavisinde kullanılabilmesinden kaynaklı iyileştirilmiş bir biyolojik aktiviteye sahip olması beklenmektedir. Buna ek olarak, kastrasyona dirençli metastatik olmayan prostat kanseri (CSMPC) tedavisinde son zamanlarda kullanılan bir ilaç olan Apalutamid (APA), zeolitik imidazolat çerçevesi-8 (ZIF-8) kullanılarak metalo kapsüllenecektir. pH'ye duyarlı bozunumu ile, yeni formülasyonun serbest çinko ve APA salınımını kanserli dokuyu sağlarken bu iki bileşenin tek bir formülasyonda birleştirilmesi sağlanacaktır. Her iki malzeme tek-kristal X-Işını kırınımı (SCXRD), toz X-ışını kırınımı (PXRD), Fourier dönüşümlü kızılötesi spektroskopisi (FTIR), termal gravimetrik analiz (TGA), diferansiyel taramalı kalorimetri (TGA ve DSC), taramalı elektron mikroskobu (SEM), yüksek performanslı sıvı kromatografisi gibi çeşitli yöntemler ile karakterize edilmiştir.

TABLE OF CONTENTS

LIST OF FIGURES

Figure **Page**

Figure **Page**

LIST OF TABLES

LIST OF ACRONYMS

API	Active Pharmaceutical Ingredient
SPX	Sparfloxacin
4-ASA	4-Aminosalicylic Acid
GRAS	Generally Regarded as Safe
SCXRD	Single Crystal X-ray Diffraction
PXRD	Powder X-ray Diffraction
FTIR	Fourier-transform Infrared Spectroscopy
FT-Raman	Fourier-transform Raman Spectroscopy
TGA	Thermogravimetric Analysis
DSC	Differential Scanning calorimetry
CSD	Cambridge Structural Database
APA	Apalutamide
SEM	Scanning Electron Microscpy
2-MeIM	2-methylimidazole
ZIF-8	Zeolitic İmidazolate Framework-8
CSMP	Castration-sensitive metastatic prostate cancer
HPLC	High Performance Liquid Chromatography
DMSO	Dimethyl sulfoxide
PBS	Phosphate-buffer saline
FDA	Food and Drug Administration

CHAPTER 1

INTRODUCTION

1.1. Crystal Engineering

Crystal Engineering is a field aiming to understand fundamental intermolecular interactions in the context of crystal packing and utilize these understanding in the design of new solids with desired chemical and physical properties.[1] Since the emerge of supramolecular chemistry, these two fields have merged and crystal engineering has been mentioned as solid-state supramolecular chemistry.[2, 3]

Over the years, crystal engineering has found its application in two main areas: gas sorption and storage for metal-organic frameworks (MOFs) and pharmaceutical polymorphs and co-crystals (organic compounds), which has contributed to continuity of the field. Apart from these two main areas, there are various application areas including catalysis, biomaterials, electronic devices. Desiraju et al. stated these five application domains of crystal engineering field[4] as illustrated in Figure 1.

1.2. Recent Advances in Crystal Engineering Related with Pharmaceutical Field

Crystal forms of active pharmaceutical ingredients (APIs), salts, hydrates, solvates and co-crystals, are majorly important in pharmaceutical industry because crystal forms have distinct advantages such as maintaining longer stability and easing the pure phase production on contrary to amorphous forms.[5] In this sense, crystal form screening of APIs has been widely implemented in pharmaceutical field.[6] In spite of certain advantages of crystal forms, they also come with certain complications such as

polymorphism, low aqueous solubility, which induces drug formulation problems.[7-9] At this point, crystal engineering provides additional perspective to cope with these problems and aims at improving the physicochemical properties of APIs including solubility, bioavailability, stability without changing the biological activity of the drug by simply altering the molecular interactions and crystal packing.[10]

Throughout the discovery of new drug, it is common to have limited physical properties such as low solubility, bioavailability and etc. In this case, salt formation of the drug is widely applied for drug with ionizable functional groups whilst co-crystal has been proposed for drug with non-ionizable functional groups.[11-14]

One of the mostly studied subclass of crystal engineering is MOFs, which was firstly introduced by O. M. Yaghi in 1995.[15] Over the years, MOFs have obtained considerable attention due to their unique properties such as high loading capacity, wide surface area, tuneable nature.[16] More particularly, MOFs have been intensively studied in drug delivery applications for the last decade as drug carriers.[17] What is more to being studied as drug carriers is that MOFs has also been proposed to be built up from endogenous metal ions and organic linkers. Furthermore, Rojas et al. states that both cation and ligand, can be bioactive in order to achieve an additive and/or a synergic therapeutic effect.[18]

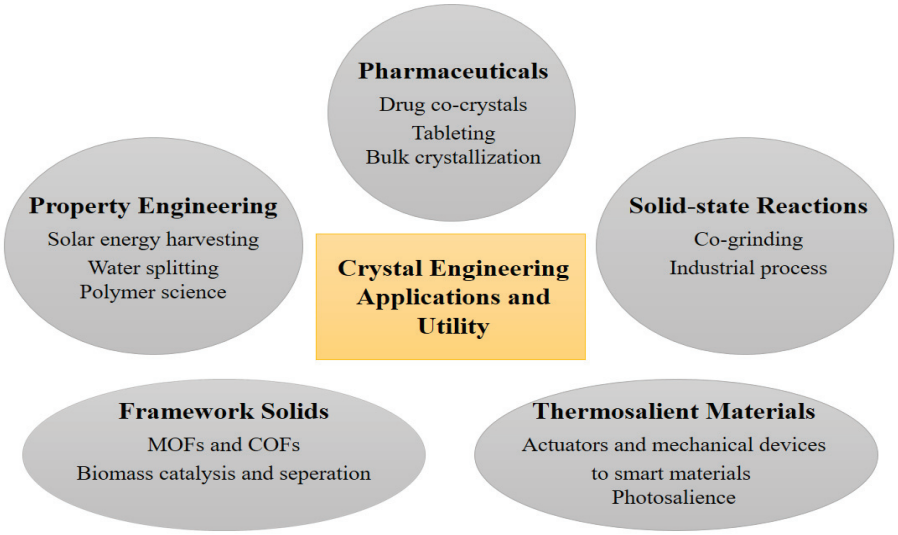

Figure 1. Five application domains of crystal engineering

CHAPTER 2

DUAL THERAPY OPPORTUNITY FOR TUBERCULOSIS

In general, co-crystal and salt screening is applied in the development stage of APIs in order to bring a solution of a problem that can be related with solid form or formulation. In addition to that, co-crystal and salt screening can also be performed in order to target solubility, dissolution rate, and bioavailability issues. In this regard, interest of API is generally combined with a co-former in the class of Generally Recognized as Safe (GRAS) substances. Subsequent to that, the new multicomponent crystals are synthesized according to crystal engineering principles. What's more up-to-date is the generation of drug-drug combination with desired properties as well as enhanced biological activity.[19, 20] In order to give a brief understanding, solid-state forms of APIs, how to design multicomponent crystal forms and synthesis methods are going to be discussed below.

2.1. Solid State Forms of Active Pharmaceutical Ingredients

In pharmaceutical science, the properties of the drug are highly related to the form of a given specific API. Along with various and diverse properties, APIs can be found in different forms like polymorphs, hydrates, solvates, salts, and co-crystals. All of these forms have different physicochemical properties, which ultimately changes the feature of APIs. Schematic representation of the multicomponent solid-state forms in pharmaceutical science is illustrated in Figure 2.

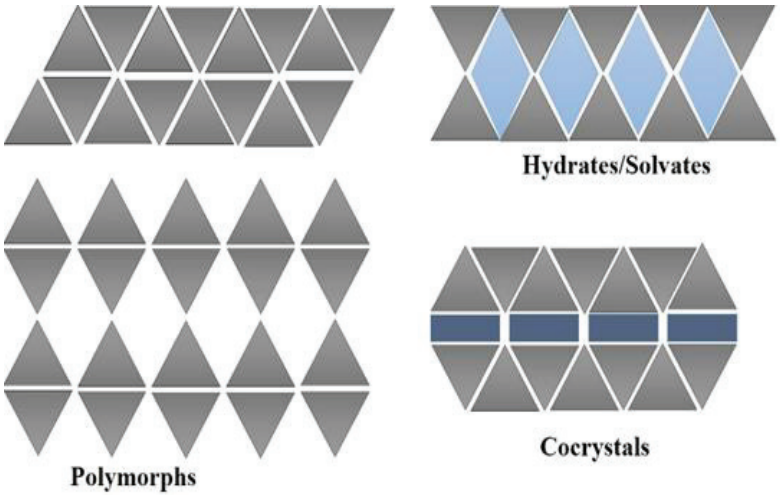

(a)

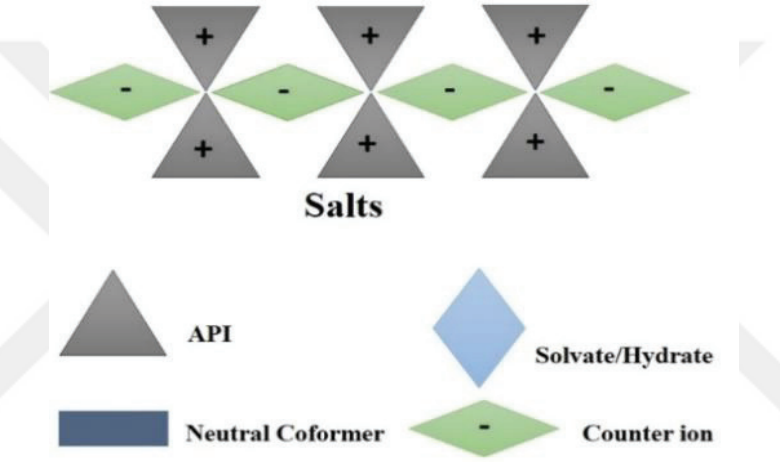

(b)

Figure 2. Schematic representation of solid forms in pharmaceutical science

Currently, it is remarkably important to be able to alter properties of the drug to enhance the behaviour and efficiency of the APIs utilized. Over the years, it has been shown that patentability and finding the most efficient forms of drugs are parallel in the research devoted to this aim. For that reason, there has been intense research regarding new forms of already known APIs, which is related to the crystal engineering field. Mostly known crystalline forms of pharmaceutical fields are mentioned below.

Polymorphism: Polymorphism refers to the tendency of compounds to exist in two or more crystalline forms whilst displaying the same chemical composition[21]. It is well-known that APIs are prone to have polymorphic forms due to the multiple active

functional groups present in their chemical structures[22]. Since the crystal lattice structure differs in polymorphic forms, inevitably, its physicochemical properties vary as well.

There are two different kinds of polymorphisms: conformation polymorphism and packing polymorphism. Conformational polymorphism occurs when there is more than one conformation in the solid-state whereas packing polymorphism occurs when more than one packing arrangement is observed, caused by different supramolecular synthons, or they possess the same supramolecular synthons but display different crystal packing.

Solvate and Hydrate: Solvate and hydrate forms of APIs are the forms in which solvent molecules are incorporated within the lattice of APIs. In the case of solvent being water, the new form is called hydrate, in other cases, it is referred as solvate[23]. Particularly, hydrate's formation is common in APIs, because they have various functional groups that are capable of acting as either hydrogen acceptors or donors for water molecules. However, solid-state phase transitions, which can possibly change the physicochemical properties of the compounds, is a great deal of issues when it comes to hydrated forms of APIs[24]

Salt: Salt formation is the most widely applied technique in order to alter and improve the physicochemical properties of APIs in the pharmaceutical field. The main reason is the ease of the procedure. In general, salt formation is dependent on the presence of ionisable groups on the API because the principle behind the formation of salt is the ionic interaction between oppositely charged molecules. Therefore, salt formation is restricted to the presence of ionisable groups in APIs. Additionally, the formation of salts can only be achieved if there are at least two or three-unit difference in pKa between the acid and the base.

Co-crystal: Over the last few years, there have been many debates related to the definition of co-crystals. With its latest accepted version by Food and Drug Administration (FDA), pharmaceutical co-crystals can be defined as crystalline materials composed of two or more different molecules, one of which is the API, in a defined stoichiometric ratio within the same crystal lattice that is associated with non-ionic and noncovalent bonds.[25]. In this regard, GRAS molecules are combined with APIs for the formation of co-crystal within in a single crystal lattice[26]. Nowadays, co-crystallization is performed with the aim of improving the physicochemical properties such as stability, dissolution, and bioavailability of APIs.[27] Furthermore, co-crystals can exist as hydrated or solvated forms likewise to APIs as well. The schematic of the co-crystal types is illustrated in Figure 3.

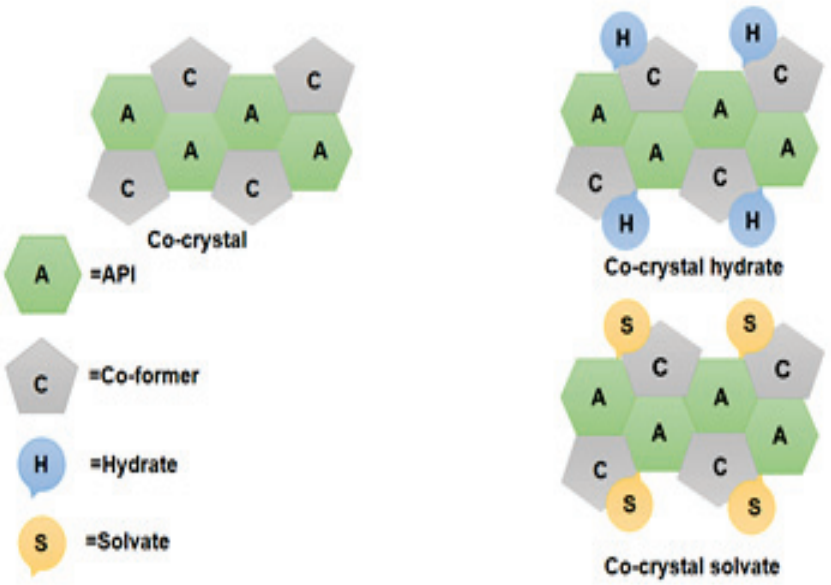

Figure 3. Schematic representation of co-crystal types in pharmaceutical science

2.2. Design of Multicomponent Crystal Forms of APIs

The design of multicomponent crystal forms of APIs requires three stages: (1) the choice of API along with a suitable co-former, (2) supramolecular synthesis, and lastly (3) the characterization of the new form. The design stages are illustrated in the schematic shown below in Figure 4.

The first step is to design. At the stage, it is necessary to specify the functional group exist in the interest of API and subsequently, make a survey[28, 29] in Cambridge Structural Database (CSD) for most probable supramolecular synthons between the potential co-former and API of interest[30].

The second step is the synthesis of the multicomponent form. Generally, polymorphic screening is the first stage of the synthesis in order to reveal probable solvate, hydrate and polymorphic forms of interest of API. Afterwards, the supramolecular synthesis is done with the use of suitable synthetic techniques. The mostly

applied synthesis strategies are reaction crystallization method, crystallization by conventional evaporation method and mechanochemistry.

The last step is the characterization of the multicomponent solid form, which requires PXRD and SCXRD, solid-state Nuclear Magnetic Resonance, FTIR, FT-Raman, TGA, and DSC[31].

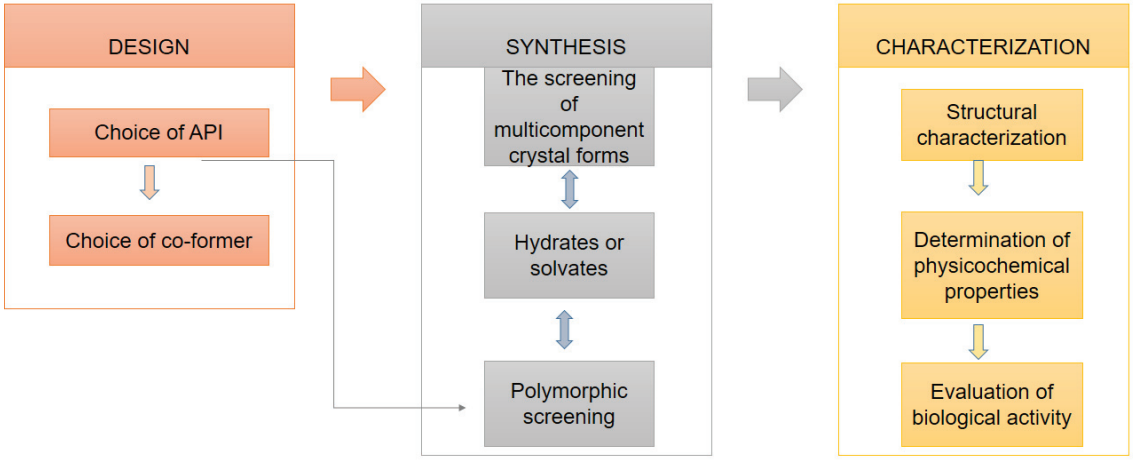

Figure 4. Schematic representation of design of multicomponent crystal froms

2.3. Methods Performed in the Synthesis of Multicomponent Forms

The formation of multicomponent forms majorly depends on the nature of the reactants and the solvent. There are various preparation methods already known in the literature such as solid-state grinding, solvent evaporation, solution crystallization, slurry conversion, melt crystallization, spray crystallization, and hot melt extrusion. In general, these synthetic methods can be divided into two categories: solid-state and solution based methods[32]. Within this chapter, solid-state grinding, solvent evaporation, and the slurry conversion is explained in detail.

Solution-based Methods

Evaporative co-crystallization: Evaporative co-crystallization is the most conventional technique when it comes to grow single crystals suitable for SXRD

measurements. The principle of this method relies on the supersaturation of the solution via evaporation, which leads to the nucleation and growth of crystals from solution. Usually, slow evaporation yields larger crystals, what is preferred. For evaporative co-crystallization, the concentration of both API and co-former have to be taken into account. In order to enlighten and guide the co-crystallization process, a few methods such as co-crystal operating range, and the analysis of ternary phase diagrams have been proposed. In spite of extra need of solvent, this technique is still the most used for industrial up-scaling processes[32].

Slurry conversion: Slurry conversion is a method in which a fixed ratio of API and co-former is put into a suspension and stirred for some hours/days. This method requires the use of excess solid fraction over solvent. The key factors of slurry conversion are solubility, the relative concentration of the compound and the co-former. Karimi-Jafari et al. stated that the transformation of co-crystal is inversely proportional to the solubility behaviour of the compounds in a specific solvent[32]. Moreover, it was also shown that the use of ternary phase diagrams can be helpful and it can be used as a guideline to optimize the reaction conditions[33].

Solid-state Methods

Mechanochemistry is broadly applied in the synthesis of new crystal forms because it offers a green alternative over conventional techniques, providing simultaneously enhanced yields.

Neat (dry) grinding: As the name implies, neat grinding involves the use of both reagents in their dry form without the use of any solvent. Either using a mortar and pestle or an automated ball mill, the reagents are subjected to pressure, which induces the formation of new multicomponent form.

Liquid-assistant grinding: Even though the principles of both grinding and liquid-assistant grinding is similar, for the application of liquid-assistant grinding, a catalytic amount of solvent is required and it can greatly facilitate the formation of new form. Yet, how the formation mechanism is induced with this technique is far from been fully understood[32, 34].

2.4. Sparfloxacin

2.4.1. Sparfloxacin

Sparfloxacin (SPX) is a broad-spectrum antimicrobial agent from the class of fluoroquinolone antibiotics, which was patented 1989[35] and launched as a medicine in 1935 for the treatment of *streptococci* and community-acquired lower respiratory tract infections[18].

As the other quinolones, the antimicrobial activity of SPX is caused by inhibition of topoisomerase II (DNA gyrase) and topoisomerase IV, which are enzymes contributing to bacterial DNA transcription, and replication[36, 37]. It possesses in vitro activity against a wide range of gram-negative and gram-positive microorganisms[38]. Compared with its counterparts in the class of fluoroquinolone antibiotics, SPX displays enhanced microbial activity against gram-positive pathogens and better in vitro activity, especially against gram-positive *cocci* and anaerobe[39, 40]. Whilst most of adverse effects are similar to other fluoroquinolones, SPX has a higher potential in phototoxicity[41, 42], for that reason, in 2001, the medicine was withdrawn from the market[43]. Furthermore, there are studies demonstrating the potent of SPX in the treatment of drug resistant tuberculosis or intolerance of first line therapy.[44-46]

From the chemistry point of view, SPX is an amphoteric drug. Its empirical formula is $C_{19}H_{22}F_2N_4O_3$ and it has the following chemical structure:

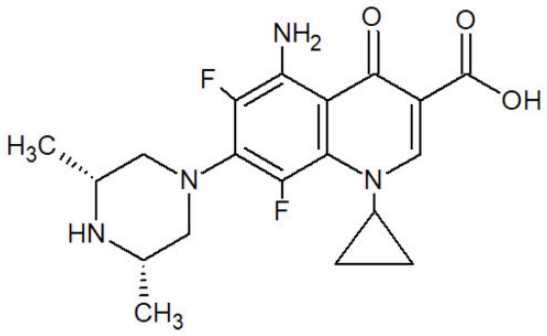

Figure 5. The molecular structure of Sparfloxacin (SPX)

Owing to its chemical structure, SPX has both a Bronsted acid (via oxoacid) and a Bronsted base (via organic amino compound) active sites. Furthermore, it is sparingly soluble in aqueous solution (0.113 mg/mL). Yet, SPX is not stable in the presence of water and immediately transforms into a hydrated form. Additionally, it can exist in both neutral and zwitterionic form. Control over these forms is highly important since they offer different properties. In general, amphoteric drugs offer a trade-off between high membrane permeability and high solubility. When the drug is available in neutral form, it has higher membrane permeability but suffers from lower solubility. On the contrary, zwitterionic forms of the drug generally tend to have higher solubility trend but poor membrane permeability, which results in limited bioavailability.

In CSD it is possible to find the crystal structure of neutral SPX, as well as two different hydrate forms [47-49]. The refcodes of thes forms are JEKMOB, COQWOU, and COQWOU01 respectively. The drug commercialized under the name of Zagam was based on SPX trihydrated form [18].

2.4.2. Literature of Sparfoxacin Multicomponent Crystal Forms

Even though there are many studies of SPX published in CSD database e.g. salt of SPX with tetrafluoroborate[50] or ionic metal complexes with zinc[51], copper[52] , there is very limited co-crystal research. Gunnam et al. showed the possible co-crystal formation between SPX and methyl, ethyl, isobutyl paraben via amino phenol synthon recognition[53]. To the best of our knowledge, there are no other studies reporting the formation of SPX multicomponent crystal forms.

2.5. 4-Aminosalicylic Acid

4-ASA is a second-line anti-tuberculosis drug that is performed for the treatment of tuberculosis.[54] The drug is mostly used with other anti-tuberculosis medicines for the treatment of all form of active tuberculosis though its use had been remained limited due

to the presence of better-tolerated antibiotics.[55] However, the drug has become one of the principal second-line anti-tuberculosis drug for the treatment of multi-drug resistant tuberculosis as well as those patients with intolerance to first-line anti-tuberculosis medications within improved formulation. [55, 56] It possesses two different antibacterial mechanism against *Mycobacterium tuberculosis* by inhibition of: (a) folic acid synthesis, (b) production of mycobactin, a cell wall substance, as a result, decreases iron intake.[57]

From chemistry point of view, 4-ASA is an amphoteric compound which can act either as a base or an acid by the presence of amino and carboxylic acid, respectively.

The CSD refcode of 4-ASA is abbreviated as AMSALA02.[58]

2.6. Work Outline and Objective

This work aims at synthesizing and characterizing multicomponent crystal forms of SPX and 4-ASA. Particularly, drug-drug combination is the main interest as alternative medicine for combined therapy since both antibiotics are demonstrated to be effective in the treatment of multi-drug resistant tuberculosis. Subsequently to the synthesis, the new multicomponent forms of SPX and 4-ASA were characterized by SCXRD, PXRD, FTIR DSC and TGA as well as the testing the stability of new forms under 78% humidity at room temperature by PXRD.

2.7. Materials and Methods

2.7.1. Materials

All the reagents and solvents were purchased from Sigma-Aldrich, Fluka, Sigma, Aldrich and Alfa Aeser and used without further purification.

2.7.2. Methods

Powder x-ray diffraction (PXRD): Samples were analysed by X-ray powder diffraction, using two diffractometers:

1) D8 Advance Bruker AXS θ-2Θ diffractometer, with a copper radiation source (Cu Kα, - λ= 1.5406 Å) and a SSD160 detector, operating at 40 kV and 30 mA. Throughout the measurements, Ni filter was used in the data collections
2) D8Advance Bruker diffractometer, with a copper radiation source (Cu Kα, λ= 1.5406 Å) and a Linxeye-XE detector, operating at 40 kV and 30 mA. Throughout the measurements, no Ni filter was used in the data collections, relying in the capability of the detector to minimize Kβ.

Single crystal x-ray diffraction (SCXRD): Suitable crystals of each co-crystals were selected and mounted on a loop with Fomblin protective oil. Data were collected on a Bruker AXS-KAPPA APEX II diffractometer and a Bruker AXS-KAPPA D8 - QUEST at 293 K, with graphite-monochromated radiation (Mo K α, λ= 0.71073 Å). The X-ray generators were operated at 50 kV and 30 mA, and the X-ray data collection was monitored by the APEX2 and APEX3 program.

Fourier transform infrared spectroscopy (FT-IR): FT-IR analysis was performed by using Nexus-Thermo Nicolet spectrometer (64 scans and resolution of 4 cm^{-1}) in the 4000−400 cm^{-1} range. Samples were prepared in KBr (1:100 in weight).

Differential scanning calorimetry (DSC) and thermogravimetric analysis (TGA): Both DSC and TGA was performed by using SETARAM TG-DTA 92 thermobalance under nitrogen flow with a heating rate of 10°C.min^{-1} for the sample (5-10 mg).

Shelf-life test: In order to investigate stability behaviour of **SPX:4ASA Form I** and **II**, 10 mg samples were placed into a desiccator with a saturated solution of NaCl (78% humidity) at room temperature. Afterward, PXRD measurements were performed once in a week for 4 weeks period of time.

Table 1. Crystallographic details of the forms of SPX:4-ASA multidrug

Structure	**SPX:4-ASA Form I**	**SPX:4-ASA Form II**
Empirical formula	$C_{26}H_{36}F_2N_5O_{14}$	$C_{13}H_{14}FN_{2.50}O_3$
Formula weight	680.60 g/mol	272.77 g/mol
Temperature	293(2) K	296(2) K
Wavelength	0.71073 Å	0.71073 Å
Limiting indices	-17<=h<=17, -39<=k<=39, -8<=l<=8	-23<=h<=23, -8<=k<=8, -26<=l<=25
Refinement method	Full-matrix least-squares on F^2	Full-matrix least-squares on F^2
Crystal system	Monoclinic	Monoclinic
Space group	*P* $2_1/c$	*P* $2_1/n$
Unit cell dimensions	a = 14.259(3) Å, b = 32.437(5) Å, c=7.1362(13) Å, α = 90º β = 98.72(5) º γ = 90º	a = 18.5866(12) Å, b = 7.1168(5) Å, c = 21.1074(13) Å, α = 90º β = 94.127(3) º γ = 90º
Volume	3262.4(10) $Å^3$	2784.8(3) $Å^3$
Z, calculated density	4, 1.386 mg/m^3	8, 1.301 mg/m^3
Reflections collected/unique	41239 / 6295 [R(int) = 0.1413]	36119 / 5709 [R(int) = 0.0674]
Data/ restraints/ parameters	6295 / 8 / 484	5709 / 6 / 378
Absorption coefficient	0.120 mm^{-1}	0.102 mm^{-1}
F (000)	1428	1144
Crystal size	0.14 x 0.08 x 0.04 mm	0.18 x 0.10 x 0.04 mm
Theta range	2.374 to 25.903º	1.410 to 26.535º
Completeness	99.9%	99.5%
R indices (all data)	R1 = 0.2105, wR2 = 0.4133	R1 = 0.1225, wR2 = 0.2532
Goodness-of-fit on F^2	1.362	1.003
Large diff. peak and hole	1.691 and -0.792 e $Å^{-3}$	0.595 and -0.306 e $Å^{-3}$
Extinction coefficient	n/a	n/a

2.8. Synthesis of SPX:4ASA Form I and II

SPX:4ASA Form I: SPX (0.0357 g) and 4-ASA (0.0142 g), corresponding to 1:1 molar ratio, was dissolved with the addition of 20 ml (1:1) EtOH: H2O solvent mixture at 50℃ for 10 minutes. Later, the solution was left to crystallize by slow evaporation of the solvent at RT. Crystals with needle shape were obtained after 3-5 days, corresponding to SPX:4ASA Form I.

Slow evaporation of SPX:4ASA Form II: SPX (0.0357 g) and 4-ASA (0.0142 g), corresponding to 1:1 molar ratio, was dissolved with the addition of 40 ml (1:1:1) EtOH:ACN:H_2O with the addition of 3 ml of NH_3 solvent mixture at 50℃ for 10 minutes. Later, the solution was left to crystallize by slow evaporation of the solvent at RT. Crystals with needle shape were obtained after 3-5 days, corresponding to SPX:4ASA Form II.

Mechanochemistry synthesis of SPX:4ASA Form II: SPX (0.0357 g) and 4-ASA (0, 0142 g), corresponding to 1:1 molar ratio, were manually grinded in a mortar with the addition of 200 µl of dimethylformamide (DMF) for 15 minutes, corresponding to SPX:4ASA Form II.

2.9. Results and Discussion

In the literature, it is possible to find examples of crystal forms that combine two different antibiotics based on the crystal engineering approach.[59] Inspired by those works, in this study, it is aimed to combine two different antibiotics, namely SPX and 4-ASA, with the hope of boosting the antimicrobial activity of the newly combined drug form.

4-ASA has three hydrogen bonding sites: aromatic carboxyl moiety, aromatic amine and hydroxyl groups, which are capable of contributing to the co-crystal or salt formation. Considering the active hydrogen bonding sites of SPX, it can be mentioned that there are probabilities of contact with all substituents present in 4-ASA. Similar to the theoretical expectations which offer salt formation due to pKa difference between

SPX[18] and 4-ASA,[54] salt formation was observed between these two drugs in the new multicomponent forms.

Throughout this study, there were two different multicomponent salts obtained. Different methods such as slow evaporation and manual grinding were applied in synthesis of these salts. Further information is given below.

2.9.1. SPX:4ASA Form I: Drug-Drug Salt

Subsequent to the synthesis of SPX:4ASA Form I, PXRD measurement was performed to assess its purity. The comparison of experimental PXRD pattern with starting reagents as well as the simulated SPX:4ASA Form I obtained from the crystal structure determined from SCXRD data is shown in Figure 6.

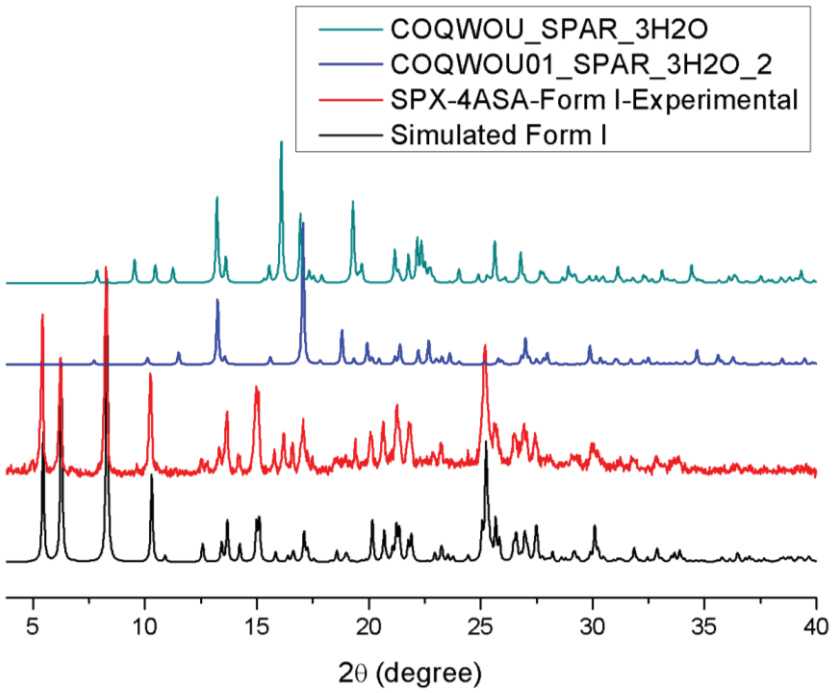

(a)

Figure 6. (Cont. on the next page)

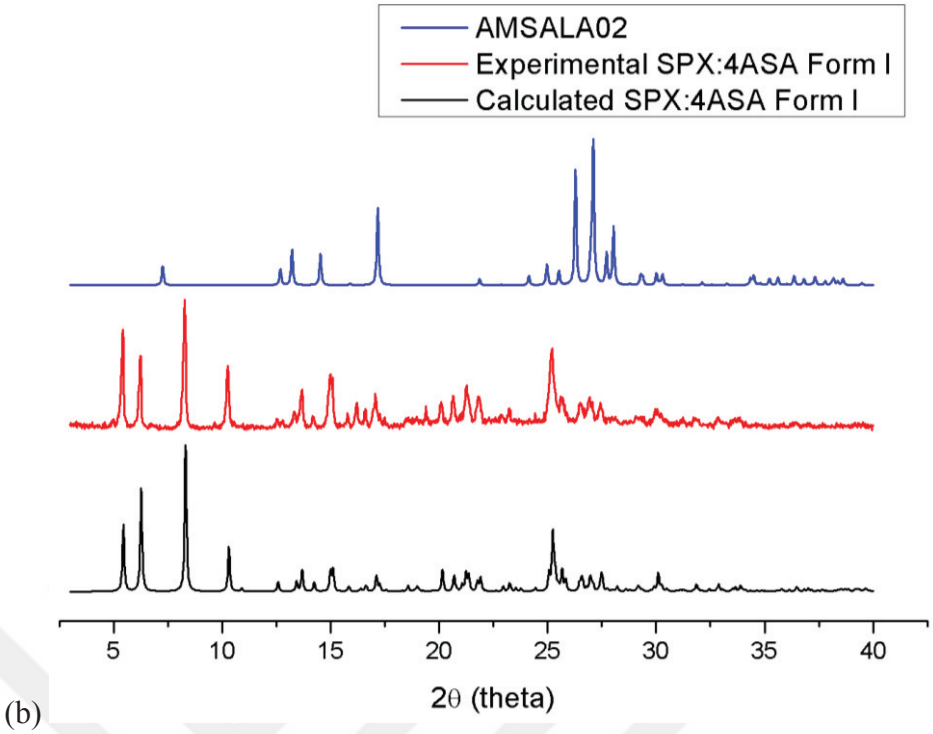

(b)

Figure 6. The comparison of experimental PXRD experimental pattern of SPX:4ASA Form I with starting reagents from (a) SPX forms (b) 4-ASA form deposited at CSD and the simulated diffractogram by SCXRD (cont.)

Based on the comparison of PXRD patterns, the formation of the new form can be stated since the experimental diffractogram is not the representative of starting reagents. Furthermore, experimental PXRD pattern is identical to the simulated SPX:4ASA Form I, which proves the formation of pure phase multicomponent form (Figure 6).

For further structural information, the result of SCXRD result, which was previously investigated within the group, is discussed below. The illustration of the asymmetric unit, the intermolecular and intramolecular interaction as well as the crystal packing of SPX:4ASA Form I are shown in Figure 7.

The asymmetric unit of SPX:4ASA Form I correspond to one cationic SPX and one anionic 4ASA and a cluster with multiple disordered water molecules. The accurate number of water molecules was not possible to confirm by SCXRD.

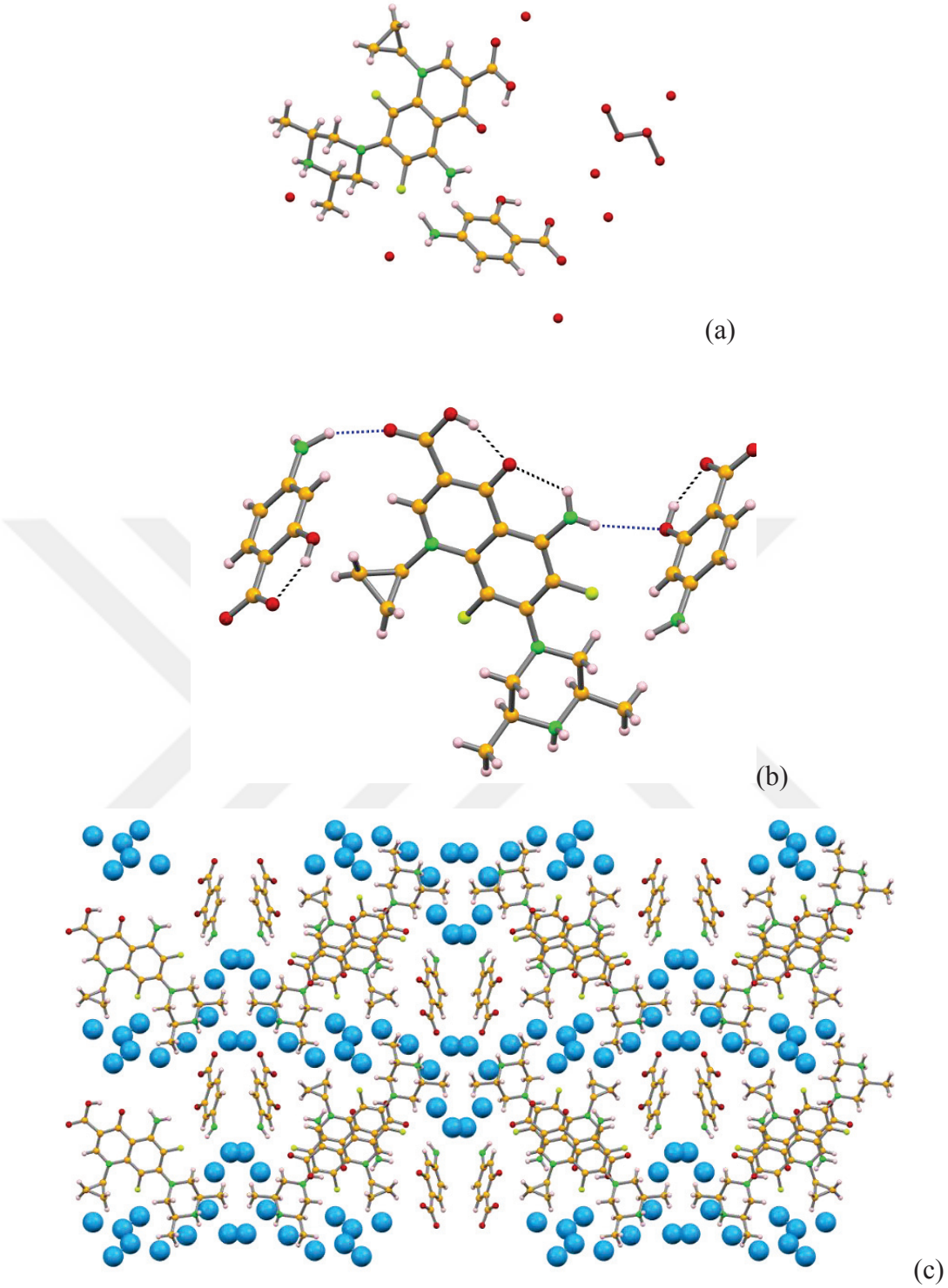

Figure 7. Illustration of SPX:4ASA Form I crystal structure depicting: (a) the asymmetric unit with the disordered water cluster; (b) the intramolecular (black) and intermolecular (blue) hydrogen bonds established between SPX and 4ASA; and (c) the crystal packing of the Form I along the *a* axis Showing the water molecules in blue and using a space fill representation

The typical intramolecular bonds in SPX established between the N-H_{NH2} and the carbonyl and the O-H_{COOH} and the carbonyl, as well as the intramolecular O-H_{COOH} ⋯ O_{OH} hydrogen bond of 4ASA are maintained. However, the N-H_{NH2} ⋯ O-H_{COOH} interactions between SPX is disrupted to give rise to interactions with 4ASA via N-$H_{NH2,SPX}$ ⋯ $O_{OH,4ASA}$ interactions.

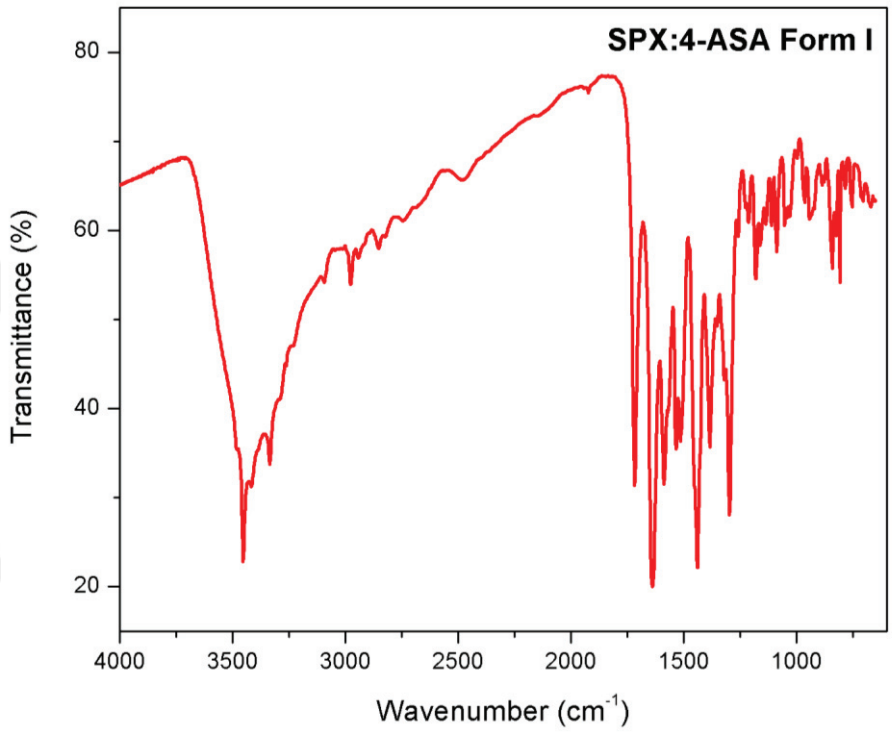

Figure 8. FT-IR spectra of SPX:4ASA Form I

The FTIR spectra of experimental SPX:4ASA Form I show the characteristic broadening around 3000 cm^{-1}, which might be attributed to the intramolecular and intermolecular hydrogen bonding of SPX:4ASA Form I. Additionally, the peak at 1537 cm^{1} is related with the amine and the C=O asymmetric stretching at 1710 cm^{-1} confirm the salt formation. Apart from those peaks, monosubstituted C=C stretching peak at 1633 cm^{-1}, C-F stretching at 1384 cm^{1} can also be found in the spectra. These peaks can be assigned to SPX whereas C-N stretching of amine at 1184 cm^{-1} can be assigned to both SPX and 4-ASA molecules (Figure 8).

2.9.2. SPX:4ASA Form II: Drug-Drug Salt

PXRD measurement was performed for the experimental powder of SPX:4ASA Form II. The PXRD comparison of the experimental procedure with the starting reagents and simulated SPX:4ASA Form II is shown in Figure 9.

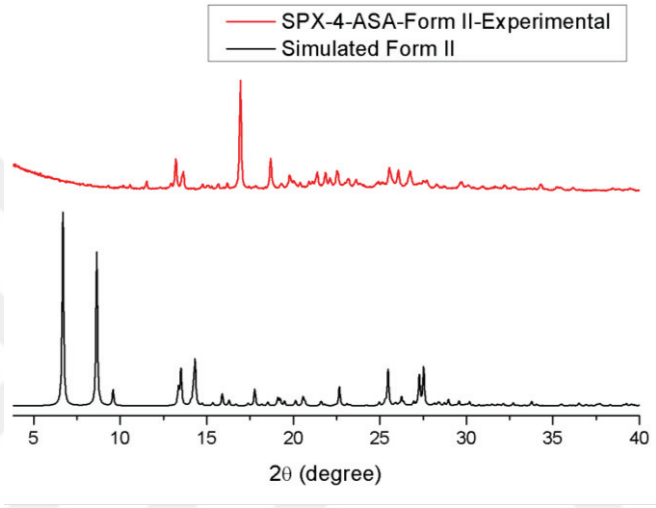

(a)

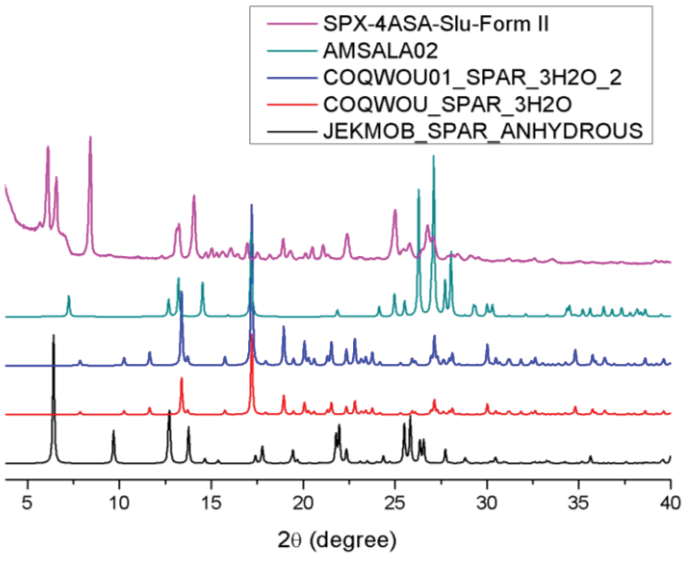

(b)

Figure 9. (Cont. on the next page)

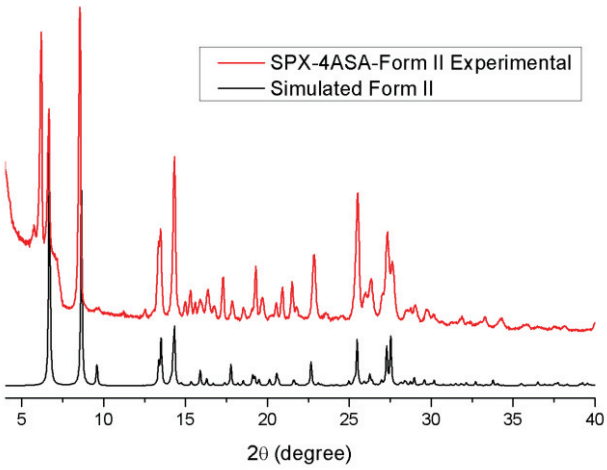

(c)

Figure 9. The comparison of the PXRD pattern of the experimental procedure of SPX:4ASA Form II with (a) starting reagents from CSD (b) SPX:4ASA Form II (c) slow evaporation versus simulated pattern from SCXRD data (cont.)

Firstly, crystal SPX:4ASA Form II was obtained by slow evaporation though PXRD measurement of experimental result indicated non-pure phase production due to the non-matching PXRD pattern of experimental and calculated result (Figure 9 (a). Bearing the unsuccessful attempts with slow evaporation method, the method was directed towards mechanochemistry in order to obtain SPX:4ASA Form II. Within the application of mechanochemistry, PXRD measurement was again performed subsequent to synthesis. According to the PXRD result with mechanochemistry, it can be mentioned that the PXRD pattern of mechanochemistry experimental procedure is different from the starting reagents (Figure 9 (b)) whereas it is almost identical to the SPX:4ASA Form II (Figure 9 (c)) except the first peak appearing in the experimental PXRD pattern. However, this one extra phase indicates impure production.

Additionally, SCXRD measurement and crystal structure solution was also performed. The illustration of the asymmetric unit, intramolecular and intermolecular interactions as well as the crystal packing of SPX:4ASA Form II is shown in Figure 10.

The asymmetric unit of SPX:4ASA Form II consists of one cationic SPX a one anionic 4ASA. The intramolecular interactions of both SPX and 4-ASA mentioned above are still maintained in the SPX:4ASA Form II**.** However, in this anhydrous form the interaction between 4ASA and SPX is established via the cationic NH_2^+ moiety of SPX.

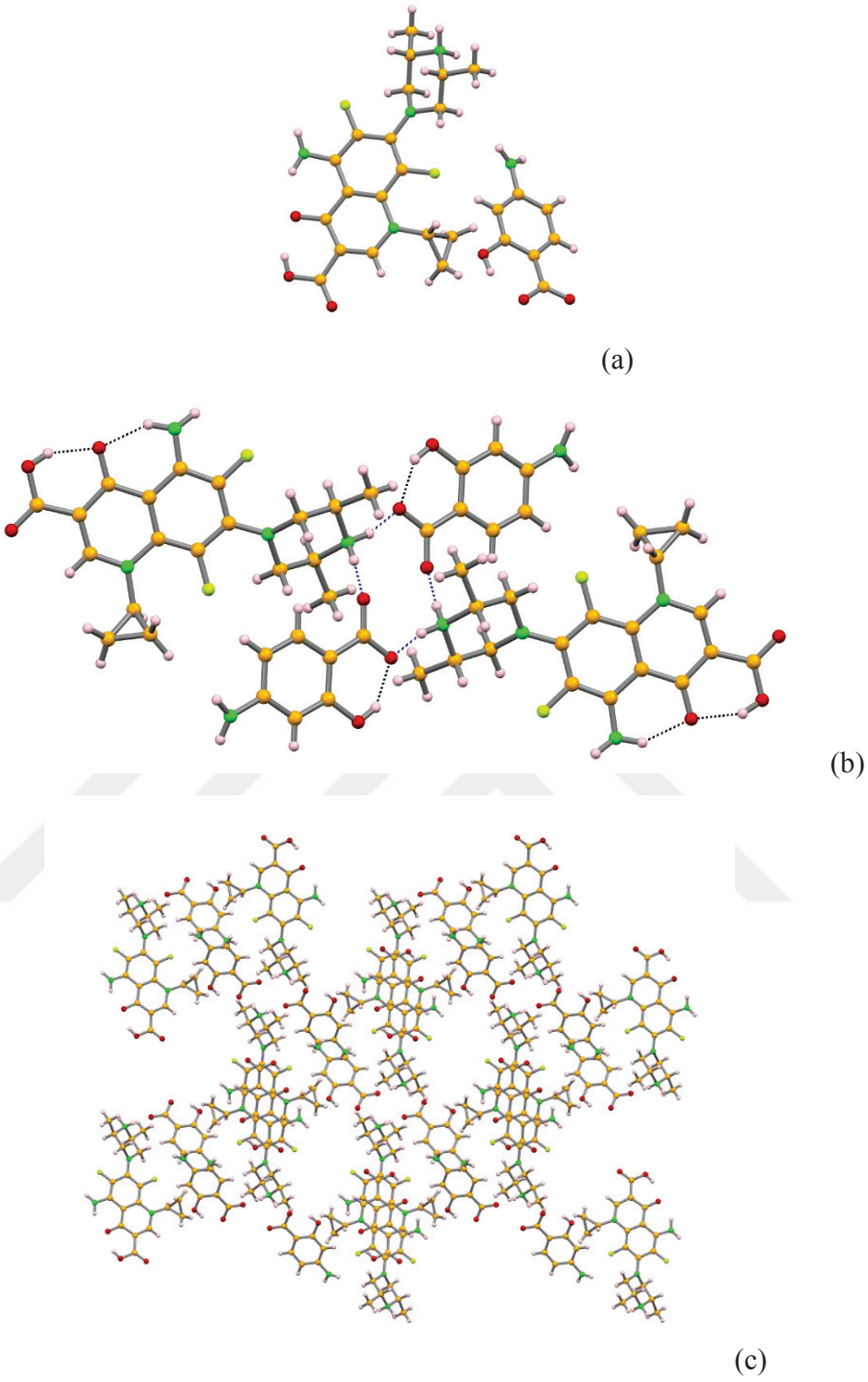

Figure 10. Illustration of SPX:4ASA Form II crystal structure depicting: (a) the asymmetric unit; (b) the intramolecular (black) and intermolecular (blue) interactions; and (c) the supramolecular arrangement in a view along the *b* axis

In a view along the *b* axis, the supramolecular arrangement shows a honey comb like packing (Figure 10 (c)). Further hydrogen bonding details of SPX:4ASA Form II are mentioned in Table 3.1.

Table 2. Hydrogen bonding details of SPX:4ASA Form II

Structure	(D)-H…A	Symmetry operator	D…A /Å	D…H /Å	H…A/ Å	D-H…A /º
SPX:4ASA Form II	N_2-H_1…O_3	x,y,z	2.639 (4)	0.90 (2)	1.87 (3)	143 (2)
	N_2-H_1…O_6	2-x, 1-y, 1-z	3.010 (4)	0.90 (2)	2.60 (4)	109 (3)
	O_2-H_{10}…O_3	x,y,z	2.506 (3)	0.82	1.75	152
	N_2-H_2…F_2	x,y,z	2.630 (4)	0.89 (3)	2.26 (4)	105 (3)
	O_6-H_6…0_5	x,y,z	2.523 (3)	0.82	1.79	147
	N_4-H_9…0_5	1/2+x, 1/2-y, -1/2+z	2.695 (4)	0.95 (3)	1.76 (3)	165 (3)
	N_4-H_{10}…0_4	3/2-x, 1/2+y, 3/2-z	2.744 (4)	0.86 (3)	1.89 (3)	175 (2)
	C_{10}-H_{10}…0_1	x,y,z	2.787 (4)	0.93	2.45	101
	C_{14}-H_{14}…F_1	x,y,z	2.724 (4)	0.97	2.49	102
	C_{14}-H_{14}…O_2	2-x, 1-y, 1-z	3.340 (4)	0.97	2.33	147
	C_{17}-H_{17}…F_2	x,y,z	2.854 (3)	0.97	2.35	113

Apart from previous structural characterization methods, FTIR measurement was also performed and the spectra of SPX:4ASA Form II is shown in Figure 11.

The FTIR spectra of SPX:4ASA Form II shows the characteristic broadening around 3000 cm-1, which might be attributed to the intramolecular and intermolecular hydrogen bonding of SPX:4ASA Form II. Additionally, the peak at 1517 cm-1 is related with the amine, as well as C=O asymmetric stretching at 1710 cm-1, proving the salt formation. Apart from those peaks, monosubstituted C=C stretching peak at 1633 cm-1, C-F stretching at 1300 cm-1 can also be found in the spectra. These peaks can be assigned to SPX whereas C-N stretching of amine at 1155 cm-1 can be assigned to both SPX and 4-ASA moieties. Furthermore, OH bending of carboxylic acid can also be found at 1436 cm^{-1} (Figure 11).

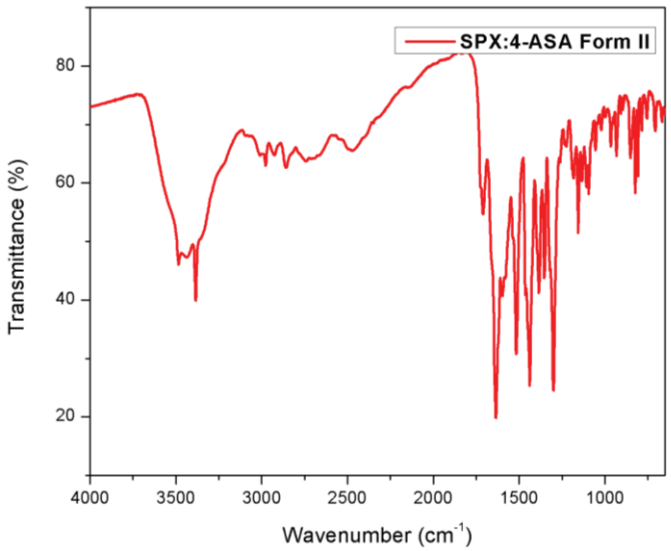

Figure 11. FTIR spectrum of SPX:4ASA Form II

Additionally, TGA-DSC measurement was also performed. The result of TGA and DSC can be found in Figure 12.

According to the DSC and TGA results, it can be stated that melting and decomposition of SPX:4ASA Form II starts at 203ºC. No mass loss is detected around 100ºC, which confirms the anhydrous nature of this form.

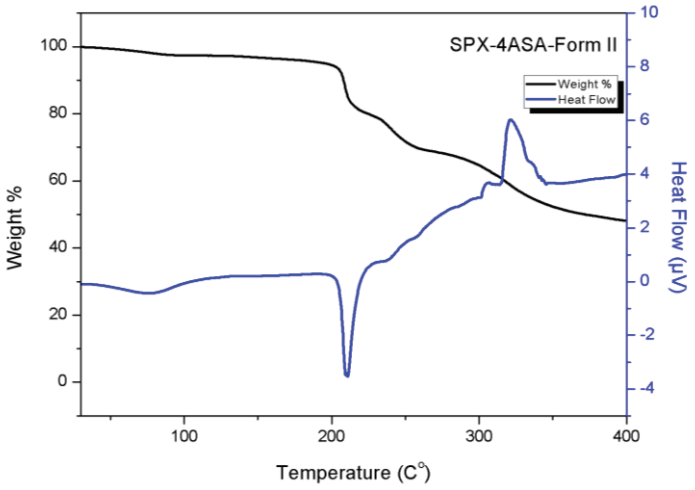

Figure 12. TGA and DSC measurement result of SPX:4ASA Form II

Shelf life

SPX:4ASA Forms I and II did not display change in PXRD diffractograms over 4 weeks under 78% room humidity for 4 weeks, which points out good stability behaviour of the new forms under the circumstances (Figure 13). Therefore, it can be stated that the new multicomponent forms of SPX and 4-ASA are stable at these conditions.

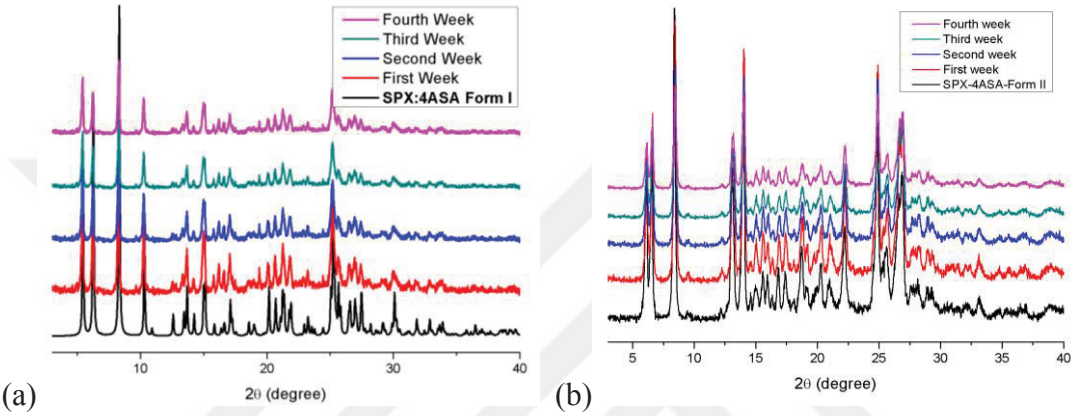

Figure 13. PXRD diffractogram comparison of (a) SPX:4ASA Form I and (b) SPX:4ASA Form II with the simulated multicomponent forms over four weeks

2.10. Conclusion

To sum up, two new multicomponent crystalline forms of SPX and 4-ASA (one molecular salt hydrate and one anhydrous molecular salt) were obtained in this study namely Form I and II and subsequently characterized by SCXRD, PXRD, TGA, DSC, and FT-IR. In these forms, it is possible to see the proton transfer from 4-ASA to SPX (piperazine ring of SPX), which led to salt formation. This result is in agreement with theoretical expectations and also literature knowledge.[60, 61]

Whilst Form I is a hydrated cluster drug-drug salt of SPX and 4-ASA, which inevitably creates a challenge to resolve full molecular structure of the new form, Form II offers an anhydrous drug-drug salt formation. It is crucial to note here that pure-phase formation of Form I was successful, yet, Form II was not obtained as a pure-phase- one

extra phase in PXRD despite to use of two different strategies, slow evaporation, and mechanochemistry, as well as alteration of synthesis parameters, time, temperature, various solvent and alteration in pH.

Studies carried out by infrared analysis have confirmed the X-ray structures of Form I and II by presenting characteristic peaks of amine salt and the C=O asymmetric stretching at 1537 cm^{1}, 1710 cm^{-1}. These peaks confirm the salt formation between SPX and 4-ASA through piperazine ring of SPX and carboxylic acid moiety of 4-ASA.

Additionally, TGA-DSC measurement pointed out the anhydrous form formation by the absence of mass loss around 100 ºC.

Shelf life studies regarding to the tolerance to 78% humidity of Form I and II proved that these forms are stable for 4 weeks under the mentioned circumstances.

Furthermore, it is noteworthy to mention that 4-ASA is an antibiotic which is used as a second line therapy medicine in multi-drug resistant tuberculosis. Likewise, there are studies demonstrating the potent of SPX in the treatment of drug resistant tuberculosis or intolerance of first line therapy. Thus, the combination of SPX and 4-ASA molecules within one crystal lattice offers a novel drug-drug therapy opportunity-alternative medicine for combined therapy, for the treatment of multi-drug resistant tuberculosis, which can possibly exhibit a superior antimicrobial activity.[44, 62] Lastly, new drug-drug molecular salts are expected to possess better solubility profile owing to salt nature.

Bringing all together, the study covers the synthesis and characterization of two different drug-drug multicomponent molecular salts. However, the investigation of these forms requires further research, time and effort, as well as the application of alternative experimental methods and conditions.

2.11. Future Perspective

In spite of current of characterizations performed within this study, there are also extra analysis needed to be performed. First of all, the pure-phase production of SPX:4ASA Form II production was unfortunately not satisfactory. In order to obtain this form as a pure phase, the use of reaction crystallization instead of slow evaporation might be an alternative approach. Asides from experimental methods, the reaction conditions

such as time, and concentration could also be critical factors. Therefore, there is a need for a more detailed and systematic approach.

Furthermore, antimicrobial activity of SPX:4ASA Form I and II is to be investigated, especially against *Mycobacterium tuberculosis*, including *in vitro* and cytotoxicity behaviour.

Lastly, kinetic solubility behaviour of SPAR:4ASA Form I, and II is to be investigated in order to display solubility profile of new forms.

CHAPTER 3

DUAL THERAPY OPPORTUNITY FOR PROSTATE CANCER

3.1. Metal-Organic Frameworks

Metal Organic-Frameworks (MOFs), organic inorganic hybrid materials, are the crystalline porous solids composed of metal ion (or metal cluster) and self-assembly polymerization of organic linker. This material class has been performed and designed for very diverse applications such as gas storage[63], separation,[64] catalysis[65], sensing[66] and drug delivery[17, 67, 68] owing to their:

1. Tailorable compositions and structures
2. Excellent porosity
3. Easier surface modification[69, 70]

Asides from other application areas, the application of biological metal-organic frameworks (BIOMOFs) is particularly interesting since it offers various advantageous:

4. Large surface area
5. Highly ordered porosities
6. Well-defined structure

In nanoscale regime, MOFs follow the ideal drug delivery requirements, large loading capacity, biocompatibility and controlled release. It possesses some advantages:

7. Versatile structure
8. High loading capacity
9. Weak coordination bonds, ensuring the biodegradability of the MOFs.

When all of these features are considered, MOFs apparently are good candidates of drug delivery.[71]

In literature, the very first BIOMOF have been studied by the use of various metal ions such as Ca, Fe, etc. and the successful BIOMOF was managed. In this studies, biology-friendly organic linkers and metal ions were chosen. Yet, it is important here that Andre et al. stated that BIOMOFs can be divided into two different groups according to the active therapeutic ingredient: (1) The organic linker, which is an endogenous linker (2) The metal ion. However, it is crucial note here that there is no BIOMOF merging the use of beneficial metal ion and organic linker to a certain disease.

3.2. Zeolitic Imidazolate Framework-8

Up till today, there have been many MOF materials which is used in drug delivery and cancer therapy. ZIF-8 is one of the most well-known and studied example of MOFs applied in drug delivery. Like inorganic zeolites, ZIF-8, made of zinc ion and 2-methylimidazole, has sodalite structure with a pore cavity of 11.6 Å and a theoretical pore aperture of 3.4 Å besides its uniform porosity and great chemical and thermal stability,[72] coming from the unique framework (Figure 14). It is not stable under acidic conditions, biodegradable, and biocompatible as well. All these feature makes ZIF-8 a very attractive drug delivery agent.

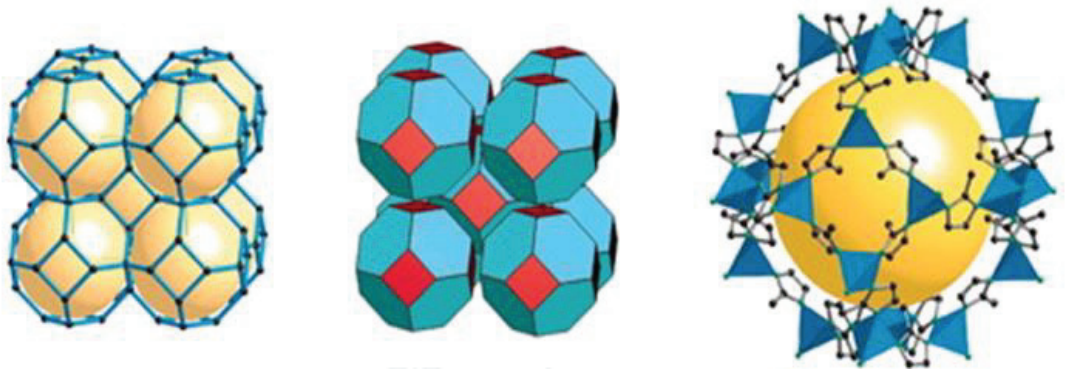

Figure 14. Topology of ZIF-8
(Source: Park, 2006)

For the first time, Park et al. stated ZIF-8 synthesis by the use dimethylformamide (DMF) as solvent.[72] Later, ZIF-8 is successfully reproduced by the use water, green biofriendly solvent.[73] Encouraged by the successful water-based synthesis, Zheng et al. showed successful encapsulation of target molecules into ZIF-8 by one-pot synthesis in aqeous medium. Nonetheless, there has been tremendous research regarding to ZIF-8 performed for encapsulation of various drugs including doxorubicin,[74] 6-mercaptopurine,[75] camptothecin[76] ,

Fluorouracil,[77] asides from caffeine,[78] insulin,[79] enzymes,[80-84] protein[85] and DNA/RNA, virus[86] Yet, there is no study in the literature which combines the therapeutic use of zinc and the encapsulated drug although ZIF-8 has been stated as potential zinc releasing container.[87]

Particularly, ZIF-8 has taken the most attention in the biological applications due to this certain property, which makes ZIF-8 pH-responsive drug delivery agent.

1. It has a high porosity yet small enterance.
2. The pH specific degradation at pH 4 and 5 whilst it displays good stability at pH 7.4. This pH intervals are particullary important because pH 7.4 is the normal pH of human body whereas lower pH is characteristic for cancerious tissues. In this regard, this MOF has been intesevely studied in the drug delivery applications.

3.3. The Relation Between Zinc and Prostate Cancer

It is known that zinc is vitally important for the human health. There are various enzymes which is catalysed by the presence of zinc ions.[88] For each cell type, there is an optimal range of total zinc concentration as well as its intracellular distribution. Any significant change in the amount of zinc results in cellular/metabolic dysfunction.

In human cells, there are two different forms of zinc: (1) tightly bound zinc occupying more than 90% of the total cellular zinc (2) loosely to moderately bind zinc, corresponding to the remaining 10%. Even though free zinc amount stays low in normal mammalian cell, the concentration is significantly higher in the male prostate cells, which indicates the metabolic importance of zinc particularly for this cell type.

There has been intense research and various supporting information regarding to the importance of free zinc ions in the prostate cancer. It has been shown that the cellular zinc levels are significantly decreased in prostate cancer, reaching to 65% with a mean standard error of <10% including *in situ* zinc staining of prostate tissue experiment. Furthermore, it is stated that the decreased zinc is an required phenomena for premalignant prostate intraepithelial neoplastic lesions and early development of malignancy.[89, 90] Moreover, the link to this decrease is stated to might have a relation with the downregulation of ZIP-1 transporter protein, which is responsible for intake of zinc ions into cell.

What is more is that there are studies illustrating the cytotoxic/tumour suppressor efficiency zinc treatment on prostate cancer.[91-93]

Regarding to decreased level of zinc and its tumour suppressor effect on prostate cancer, Costello et al. mention that "This relationship provide the basis and the opportunities for the potential development of zinc-associated chemotherapeutic agents.[93]"

3.4. Apalutamide

In prostate cancer treatment, the first-line therapy option is androgen-deprivation therapy[94] though patients becomes resistant to this therapy (castration-resistant prostate cancer) inevitably[95] due to persistent active AR signalling by amplified AR gene and overexpression of AR.[96, 97] Hence, AR inhibitors which blocks the AR signalling are offered for the treatment of castration-resistant prostate cancer (CRPC).[95, 98]

APA is a new generation AR inhibitor drug which is launched under the name of Erleda and also the first FDA-approved drug used in the treatment of castration-resistant non-metastatic prostate cancer.[98] It inhibits AR nuclear translocation, DNA binding and transcription of AR gene targets in prostate tumours. APA displays better androgen inhibition compared with other androgen inhibitors. Koukourakis et al. showed that APA was more effective on cell proliferation by blocking the AR route better than bicalutamide in normoxia and hypoxia conditions[99]. In another study, although APA and bicalutamide were bound to the same ligand binding site, Apalutamide was reported to be more effective by binding to the AR receptor with an affinity between seven and tenfold higher.[98]

3.5. Work Outline and Objective

Costello et al. states:

> "For prostate cancer, the key issue is to deliver zinc into ZIP1-deficient malignant cells and increase the cellular level of mobile reactive zinc, which will manifest the cytotoxic/tumor suppressor effect of zinc".[93]

Inspired by his research outcomes, this work aims at verifying the potential of ZIF-8 as zinc-releasing agent in CSMPC. In this sense, APA, as a new promising medicine in CSMPC is going to be encapsulated by ZIF-8 using one-pot synthesis taken the basis from Kaur et al.'s work (Figure 15). As a result, a formulation for combined therapeutic effect of zinc ions and APA is going to be established and the zinc and APA releasing behaviour of this new formulation is going to be evaluated.

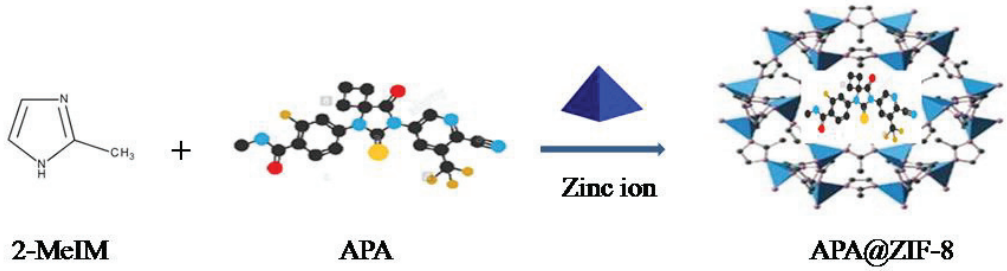

Figure 15. One-pot synthesis of APA@ZIF-8

This work aims to verify the potential of ZIF-8 as zinc-releasing agent in prostate cancer. In this sense, APA is going to be encapsulated by ZIF-8, therefore, a formulation for combined the therapeutic effect of zinc ions and APA is going to be established.

3.6. Materials and Methods

3.6.1. Materials

All the reagents and solvents were purchased from Sigma-Aldrich, Fluka, Sigma, Aldrich and Alfa Aeser and used without further purification**.**

3.6.2. Methods

Powder x-ray diffraction (PXRD): Samples were analysed by X-ray powder diffraction Philips Xarakpert Pro diffractometer, with a copper radiation source (Cu Kα, - λ= 1.5406 Å), with a beam length at 40 kV and 25 mA. Throughout the measurements, Ni filter was used in the data collections

Fourier transform infrared spectroscopy (FT-IR): FT-IR analysis was performed by using Perkin Elmer FT-IR System Spectrum BX in the 4000−400 cm^{-1} range. Samples were prepared in KBr (1:100 in weight).

Scanning electron microscopy: Scanning electron microscope was performed using the 5 kV accelerating voltage by using the FEI QUANTA 250 FEG device. The samples were be sputter-coated with gold.

High performance liquid chromatography: Apalutamide were assayed using Agilent 1100 Series occupied with an auto-sampler and photo diode array (PDA) detector set at λ_{max} 260.4 nm for quantitation of the analytes. The chromatographic separation was achieved on C18 column maintained at 30°C. The binary mobile phase system consisted of reservoir A (0.095% trifluoroacetic acid (TFA) in acetonitrile) and reservoir B (0.1% TFA in water) were run as per the flow regulated gradient program given below. The injection volume was 10 µL.

Table 3. HPLC details for the quantitative determination of Apalutamide

Time (min)	Flow rate (ml/min)	Mobile Phase A (0.095% TFA in ACN) (%)	Mobile Phase B (0.1% TFA in H_2O) (%)
0	1	5	95
2	1	20	80
4	1	95	5
7	1	95	5
8	1	5	95
15	1	5	95

3.7. APA@ZIF-8 Synthesis

In order to synthesis both ZIF-8 and APA@ZIF-8, the one-pot synthesis method developed by Kaur et. al.[75] According to the synthesis details, 1.135 g of 2-MeIM is placed into a vial and dissolved with addition of 4 ml of water for 5 minutes with accompanied stirring. Later on, 58.5 mg of $Zn(NO_3)_2$ $6H_2O$ is put and dissolved in another via with 400µL water. In the meantime, 6 mg of APA is placed into an eppendorf and dissolved with the addition of 600 µL of dimethyl sulfoxide (DMSO). This step is replaced with just addition of 600 µL of DMSO for ZIF-8 synthesis. Afterwards, the solution containing APA is transferred into vial containing 2-MeIM. Then, this solution containing both APA and 2-MeIM is poured drop by drop to the solution containing $Zn(NO_3)_2$ $6H_2O$ and the solution is stirred for 15 minutes. Lastly, the solution is transferred into eppendorfs and centrifugated for 15 minutes at 14000 rpm. The nanoparticles are washed with 30:70 EtOH:H_2O three times and placed into oven at 65ºC for dry.

3.8. Results and Discussion

Firstly, the formation of ZIF-8 and APA@ZIF-8 was investigated by PXRD measurement. The PXRD result is illustrated in Figure 16. The results indicated the

presence of characteristic peaks of ZIF-8 at 7.34, 10.46, 12.79, 14.75, 16.53, 18.12, 22.21, 24.56, 26.77, 29.76, 30.67, 31.62, 32.46 theta degree both in ZIF-8 and APA@ZIF-8 corresponding to (011), (002), (112), (022), (013), (222), (114), (233), (134), (044), (334), (244), (235) indices, respectively. The result shows the successful synthesis of ZIF-8 and APA@ZIF-8. Noteworthy to mention that both diffractograms are in agreement with literature knowledge.[72]

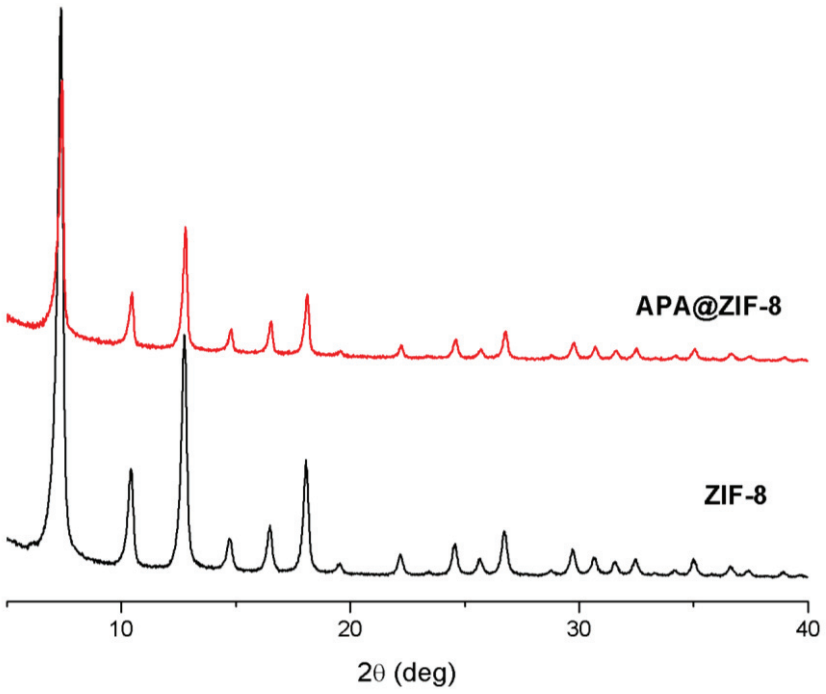

Figure 16. PXRD patterns of both ZIF-8 and APA@ZIF-8

Afterwards, SEM images of ZIF-8 and APA@ZIF-8 were taken. Based on the SEM, it is possible to conclude the formation of hexagonal shape nanoparticles, which is characteristic for ZIF-8. Additionally, the size of ZIF-8 was found to be 120 ± 50 nm whilst APA@ZIF-8 was 200 ± 50 nm (Figure 17). It is important to note there that the size and shape of the nanoparticles are in agreement with other ZIF-8 and drug-loaded ZIF-8 nanoparticles known in the literature.[75]

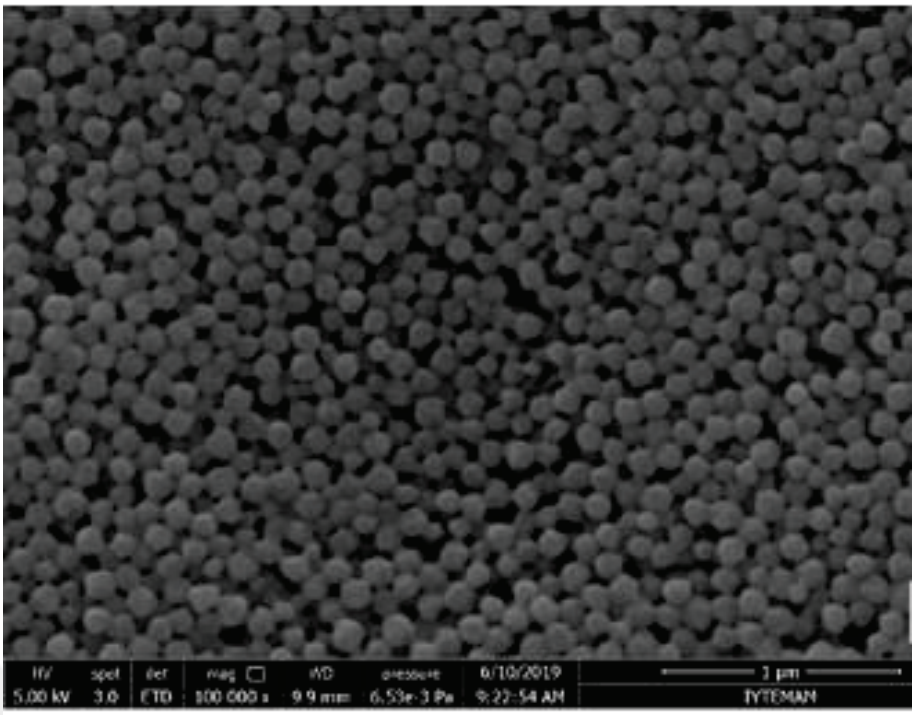

(a)

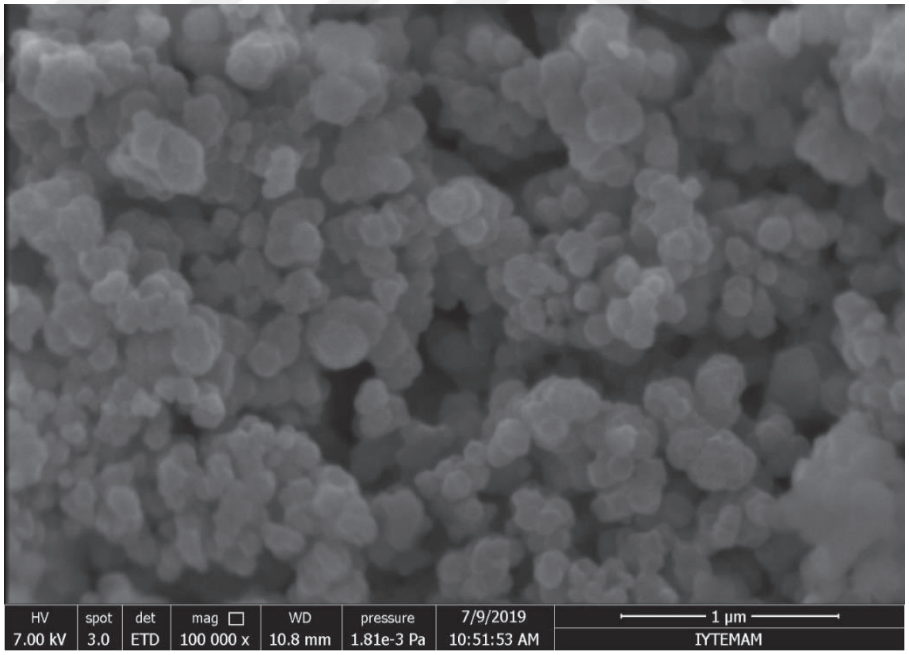

(b)

Figure 17. SEM image of (a) ZIF-8 (b) APA@ZIF-8

Furthermore, FT-IR measurement was performed for APA, ZIF-8 and APA@ZIF-8 nanoparticles. In general, there is neither difference between FT-IR spectra of ZIF-8 and APA@ZIF-8 nor overlapping of FTIR spectra of APA and APA@ZIF-8. This result suggests the successful incorporation of APA into ZIF-8 molecules rather than direct interaction with zinc or 2-MeIM. Having a closer look at the spectra of both ZIF-8 and APA@ZIF-8, strong bands at 1448 cm^{-1}, 1429 cm^{-1}, 1311 cm^{-1}, 1149 cm^{-1}, 754 cm^{-1} can be seen asides from moderate peaks at 1184 cm^{-1}, 998 cm^{-1}, 691 cm^{-1}, and weak peaks at 1587 cm^{-1} and 962 cm^{-1} (Figure 18). These results are in good agreement with literature knowledge.[72]

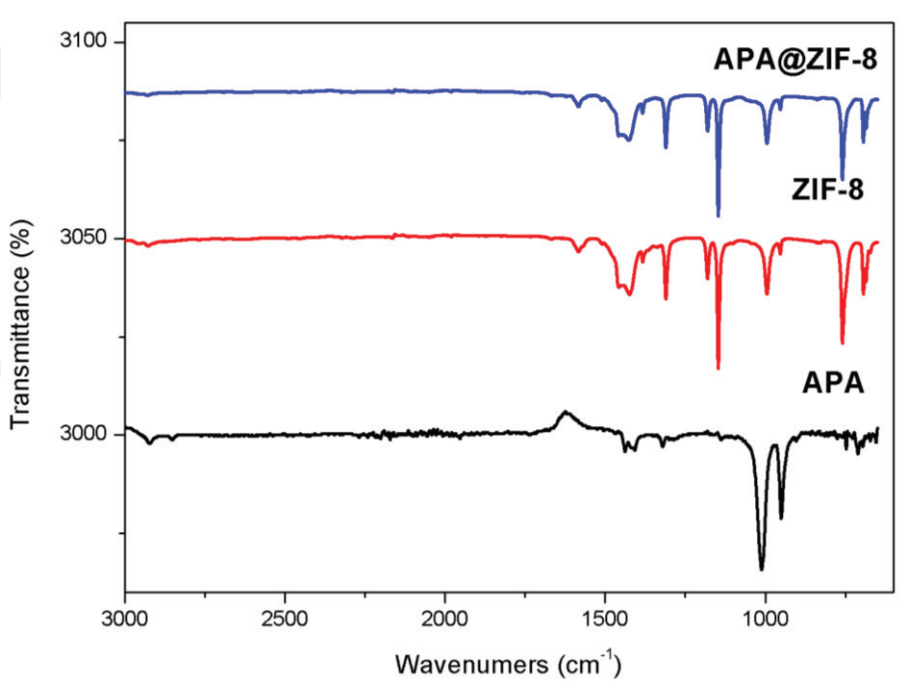

Figure 18. The comparison of FT-IR spectra of APA, experimental ZIF-8 and APA@ZIF-8

Subsequently, the loading efficiency of the APA@ZIF-8 was determined by HPLC method using the following equation:

$$Loading\ efficiency\ (\%) = \frac{Rxn\ medium\ conc. - supernatant\ conc.}{Rxn\ medium\ conc.} \times 100$$

According to the HPLC calibration curve, the concentration of reaction supernatant found to be 277.05 ppm, which ultimately results in 76.91% loading efficiency of total drug into APA@ZIF-8. This result shows 4.62 mg APA the loading into APA@ZIF-8. The standard curve of APA and loading efficiency is shown in Appendix A.

3.9. Conclusion

To sum up, this study demonstrated the synthesis of ZIF-8 and APA@ZIF-8 in following to that the nanoparticles were characterized by various methods such as PXRD, SEM, FT-IR, and HPLC. Furthermore, the characterization results are in agreement with literature.

PXRD diffractograms showed no structural difference between ZIF-8 and APA@ZIF-8, and also literature information which points out successful pure-phase production. Additionally, FT-IR spectra also proved the equal experimental spectra when it is compared with literature information. Lastly, the shape of ZIF-8 and APA@ZIF-8 nanoparticles were investigated by SEM. All of these characterization methods proved successful formation of both ZIF-8 and APA@ZIF-8.

Furthermore, drug loading efficiency of APA@ZIF-8 was found to be 76.91%, which ultimately results in 4.62 mg of APA encapsulation into APA@ZIF-8.

Bringing all together, a new synergetic therapeutic formulation which combines free zinc ions and APA for the treatment of CSMPC was successfully accomplished and characterized.

3.10. Future Perspective

In spite of current of characterizations performed within this study, there are also extra analysis needed to be performed. First of all, drug release profile at pH 5 and 7.4 is needed to be investigated over time in order to verify and demonstrate drug release

profiles. Additionally, the potent of both ZIF-8 and APA@ZIF-8 should be investigated within *in vitro* test such as cytotoxicity and cell viability of prostate cancer cell lines such as PC3, LNCAP and RWPE1 asides from other analyses such as apoptosis, western-blot analysis and etc. Following with in vitro analysis, APA@ZIF-8 nanoparticles should be tested *in vivo* and *ex vivo*.

REFERENCES

1. Desiraju, G. R.; Parshall, G. W., Crystal engineering: the design of organic solids. *Materials science monographs* **1989,** *54*.

2. Soldatov, D.; Terekhova, I., Supramolecular chemistry and crystal engineering. *Journal of Structural Chemistry* **2005,** *46* (1), S1-S8.

3. Nangia, A., Supramolecular chemistry and crystal engineering. *Journal of chemical sciences* **2010,** *122* (3), 295-310.

4. Nangia, A. K.; Desiraju, G. R., Crystal Engineering: An Outlook for the Future. *Angewandte Chemie International Edition* **2019,** *58* (13), 4100-4107.

5. Mukherjee, S., Crystal engineering of pharmaceutical cocrystals. **2011**.

6. Allen, L. V.; Popovich, N. G.; Ansel, H. C., Pharmaceutical dosage forms and drug delivery systems. *Delhi, India: BI Pubication* **2005,** *8*, 265.

7. Brittain, H. G., Theory and principles of polymorphic systems. *Polymorphism in Pharmaceutical Solids* **2009,** *192*, 1.

8. Brittain, H. G., Polymorphism and solvatomorphism 2010. *Journal of pharmaceutical sciences* **2012,** *101* (2), 464-484.

9. Bernstein, J.; Bernstein, J. M., *Polymorphism in molecular crystals*. Oxford University Press: 2002; Vol. 14.

10. Almarsson, Ö.; Zaworotko, M. J., Crystal engineering of the composition of pharmaceutical phases. Do pharmaceutical co-crystals represent a new path to improved medicines? *Chemical communications* **2004,** (17), 1889-1896.

11. Stahl, P.; Wermuth, C., Handbook of Pharmaceutical Salts: Properties, Selection, and Use. Weily-VCH: Zurich, 1-7, 2002.(b) Gould. *PJ Int. J. Pharm* **1986,** *33*, 201-217.

12. Brittain, H. G., Polymorphism: pharmaceutical aspects. *Encyclopedia of Pharmaceutical Technology* **2002,** *3*, 2239-2249.

13. Berge, S. M.; Bighley, L. D.; Monkhouse, D. C., Pharmaceutical salts. *Journal of pharmaceutical sciences* **1977,** *66* (1), 1-19.

14. Giron, D.; Mutz, M.; Garnier, S., Solid-state of pharmaceutical compounds. *Journal of thermal analysis and calorimetry* **2004,** *77* (2), 709-747.

15. Yaghi, O. M.; Li, G.; Li, H., Selective binding and removal of guests in a microporous metal–organic framework. *Nature* **1995,** *378* (6558), 703

.

16. Motkuri, R. K.; Liu, J.; Fernandez, C. A.; Nune, S. K.; Thallapally, P.; McGrail, B. P., Metal organic frameworks-synthesis and applications. *Industrial Catalysis and Separations* **2014**, 61-103.

17. Cao, J.; Li, X.; Tian, H., Metal-Organic Framework (MOF)-Based Drug Delivery. *Current Medicinal Chemistry* **2019**.

18. Rojas, S.; Devic, T.; Horcajada, P., Metal organic frameworks based on bioactive components. *Journal of Materials Chemistry B* **2017,** *5* (14), 2560-2573.

19. Thakuria, R.; Sarma, B., Drug-drug and drug-nutraceutical cocrystal/salt as alternative medicine for combination therapy: a crystal engineering approach. *Crystals* **2018,** *8* (2), 101.

20. Putra, O. D.; Furuishi, T.; Yonemochi, E.; Terada, K.; Uekusa, H., Drug–drug multicomponent crystals as an effective technique to overcome weaknesses in parent drugs. *Crystal Growth & Design* **2016,** *16* (7), 3577-3581.

21. Mullin, J. W., *Crystallization*. Elsevier: 2001.

22. Guranda, D.; Deeva, G., Drug synthesis methods and manufacturing technologies. *Pharm Chem J* **2010,** *44*, 22-28.

23. Healy, A. M.; Worku, Z. A.; Kumar, D.; Madi, A. M., Pharmaceutical solvates, hydrates and amorphous forms: A special emphasis on cocrystals. *Advanced drug delivery reviews* **2017,** *117*, 25-46.

24. Clarke, H. D. M., Crystal Engineering of Multi-Component Crystal Forms: The Opportunities and Challenges in Design. **2012**

.

25. Health, U. D. o.; Services, H.; Food; Administration, D., Regulatory classification of pharmaceutical co-crystals: Guidance for industry. *Center for Drug Evaluation and Research (CDER), Silver Spring, US* **2018**.

26. Mukherjee, A., Building upon supramolecular synthons: some aspects of crystal engineering. *Crystal Growth & Design* **2015,** *15* (6), 3076-3085.

27. Schultheiss, N.; Newman, A., Pharmaceutical cocrystals and their physicochemical properties. *Crystal growth and design* **2009,** *9* (6), 2950-2967.

28. Miroshnyk, I.; Mirza, S.; Sandler, N., Pharmaceutical co-crystals–an opportunity for drug product enhancement. *Expert opinion on drug delivery* **2009,** *6* (4), 333-341.

29. Qiao, N.; Li, M.; Schlindwein, W.; Malek, N.; Davies, A.; Trappitt, G., Pharmaceutical cocrystals: an overview. *International journal of pharmaceutics* **2011,** *419* (1-2), 1-11.

30. Desiraju, G. R., Supramolecular synthons in crystal engineering—a new organic synthesis. *Angewandte Chemie International Edition in English* **1995,** *34* (21), 2311-2327.

31. Domingos, S.; André, V.; Quaresma, S.; Martins, I. C.; Minas da Piedade, M. F.; Duarte, M. T., New forms of old drugs: improving without changing. *Journal of Pharmacy and Pharmacology* **2015,** *67* (6), 830-846.

32. Karimi-Jafari, M.; Padrela, L.; Walker, G. M.; Croker, D. M., Creating cocrystals: a review of pharmaceutical cocrystal preparation routes and applications. *Crystal Growth & Design* **2018,** *18* (10), 6370-6387.

33. Jayasankar, A.; Reddy, L. S.; Bethune, S. J.; Rodríguez-Hornedo, N., Role of cocrystal and solution chemistry on the formation and stability of cocrystals with different stoichiometry. *Crystal Growth and Design* **2009,** *9* (2), 889-897.

34. Do, J.-L.; Friščić, T., Mechanochemistry: a force of synthesis. *ACS central science* **2016,** *3* (1), 13-19.

35. Matsumoto, J.-i.; Miyamoto, T.; Egawa, H.; Nakamura, S., 5-substituted-6, 8-difluoroquinolines useful as antibacterial agents. Google Patents: 1989.

36. Andersson, M. I.; MacGowan, A. P., Development of the quinolones. *Journal of Antimicrobial Chemotherapy* **2003,** *51* (suppl_1), 1-11.

37. Suh, B.; Lorber, B., Quinolones. *Medical Clinics of North America* **1995,** *79* (4), 869-894.

38. Wolfson, J. S.; Hooper, D. C., The fluoroquinolones: structures, mechanisms of action and resistance, and spectra of activity in vitro. *Antimicrobial agents and Chemotherapy* **1985,** *28* (4), 581.

39. Miyamoto, T.; Matsumoto, J.-i.; Chiba, K.; Egawa, H.; Shibamori, K.; Minamida, A.; Nishimura, Y.; Okada, H.; Kataoka, M.; Fujita, M., Synthesis and structure-activity relationships of 5-substituted 6, 8-difluoroquinolones, including sparfloxacin, a new quinolone antibacterial agent with improved potency. *Journal of medicinal chemistry* **1990,** *33* (6), 1645-1656.

40. Nakamura, S.; Minami, A.; Nakata, K.; Kurobe, N.; Kouno, K.; Sakaguchi, Y.; Kashimoto, S.; Yoshida, H.; Kojima, T.; Ohue, T., In vitro and in vivo antibacterial activities of AT-4140, a new broad-spectrum quinolone. *Antimicrobial agents and chemotherapy* **1989,** *33* (8), 1167-1173.

41. Pierfitte, C.; Royer, R. J.; Moore, N.; Bégaud, B., The link between sunshine and phototoxicity of sparfloxacin. *British journal of clinical pharmacology* **2000,** *49* (6), 609-612.

42. Gibbs, N. K., Drug-induced skin phototoxicity: lessons from the fluoroquinolones. In *Comprehensive Series in Photosciences*, Elsevier: 2001; Vol. 3, pp 337-356.

43. Outterson, K.; Powers, J. H.; Seoane-Vazquez, E.; Rodriguez-Monguio, R.; Kesselheim, A. S., Approval and withdrawal of new antibiotics and other antiinfectives in the US, 1980–2009. *The Journal of Law, Medicine & Ethics* **2013,** *41* (3), 688-696.

44. Lubasch, A.; Erbes, R.; Mauch, H.; Lode, H., Sparfloxacin in the treatment of drug resistant tuberculosis or intolerance of first line therapy. *European Respiratory Journal* **2001,** *17* (4), 641-646.

45. Lourenço, M.; Junior, I. N.; De Souza, M., In vitro activity of ciprofloxacin, ofloxacin, levofloxacin, sparfloxacin and gatifloxacin against multidrug-resistant Mycobacterium tuberculosis in Rio de Janeiro Brazil. *Médecine et maladies infectieuses* **2007,** *5* (37), 295-296.

46. Klemens, S.; DeStefano, M.; Cynamon, M., Therapy of multidrug-resistant tuberculosis: lessons from studies with mice. *Antimicrobial agents and chemotherapy* **1993,** *37* (11), 2344-2347.

47. Miyamoto, T.; Matsumoto, J.; Chiba, K.; Egawa, H.; Shibamori, K.; Minamida, A.; Nishimura, Y.; Okada, H.; Kataoka, M., Pyridonecarboxylic acids as antibacterial agents. Part 14. Synthesis and structure-activity relationships of 5-substituted 6, 8-difluoroquinolones, including sparfloxacin, a new quinolone

antibacterial agent with improved potency. *Journal of Medicinal Chemistry* **1990,** *33* (6), 1645-1656.

48. Sivalakshmidevi, A.; Vyas, K.; Om Reddy, G., Sparfloxacin, an antibacterial drug. *Acta Crystallographica Section C: Crystal Structure Communications* **2000,** *56* (3), iuc0000046-e116.

49. Llinàs, A.; Burley, J. C.; Prior, T. J.; Glen, R. C.; Goodman, J. M., Concomitant hydrate polymorphism in the precipitation of sparfloxacin from aqueous solution. *Crystal Growth and Design* **2008,** *8* (1), 114-118.

50. Shingnapurkar, D.; Butcher, R.; Afrasiabi, Z.; Sinn, E.; Ahmed, F.; Sarkar, F.; Padhye, S., Neutral dimeric copper–sparfloxacin conjugate having butterfly motif with antiproliferative effects against hormone independent BT20 breast cancer cell line. *Inorganic Chemistry Communications* **2007,** *10* (4), 459-462.

51. Vasiliev, A.; Golovnev, N., Crystal structure of two ionic sparfloxacin compounds. *Journal of Structural Chemistry* **2015,** *56* (5), 907-911.

52. Efthimiadou, E. K.; Sanakis, Y.; Raptopoulou, C. P.; Karaliota, A.; Katsaros, N.; Psomas, G., Crystal structure, spectroscopic, and biological study of the copper (II) complex with third-generation quinolone antibiotic sparfloxacin. *Bioorganic & medicinal chemistry letters* **2006,** *16* (14), 3864-3867.

53. Gunnam, A.; Suresh, K.; Ganduri, R.; Nangia, A., Crystal engineering of a zwitterionic drug to neutral cocrystals: a general solution for floxacins. *Chemical Communications* **2016,** *52* (85), 12610-12613.

54. Lehmann, J., Twenty years afterward: historical notes on the discovery of the antituberculosis effect of para-aminosalicylic acid (PAS) and the first clinical trials. American Lung Association: 1964.

55. Parvez, M. M.; Shin, H. J.; Jung, J. A.; Shin, J.-G., Evaluation of para-aminosalicylic acid as a substrate of multiple solute carrier uptake transporters

and possible drug interactions with nonsteroidal anti-inflammatory drugs in vitro. *Antimicrobial agents and chemotherapy* **2017,** *61* (5), e02392-16.

56. Rengarajan, J.; Sassetti, C. M.; Naroditskaya, V.; Sloutsky, A.; Bloom, B. R.; Rubin, E. J., The folate pathway is a target for resistance to the drug para-aminosalicylic acid (PAS) in mycobacteria. *Molecular microbiology* **2004,** *53* (1), 275-282.

57. Minato, Y.; Thiede, J. M.; Kordus, S. L.; McKlveen, E. J.; Turman, B. J.; Baughn, A. D., Mycobacterium tuberculosis folate metabolism and the mechanistic basis for para-aminosalicylic acid susceptibility and resistance. *Antimicrobial agents and chemotherapy* **2015,** *59* (9), 5097-5106.

58. Montis, R.; Hursthouse, M. B., Surprisingly complex supramolecular behaviour in the crystal structures of a family of mono-substituted salicylic acids. *CrystEngComm* **2012,** *14* (16), 5242-5254.

59. Tyers, M.; Wright, G. D., Drug combinations: A strategy to extend the life of antibiotics in the 21st century. *Nature Reviews Microbiology* **2019**, 1.

60. Reddy, J. S.; Ganesh, S. V.; Nagalapalli, R.; Dandela, R.; Solomon, K. A.; Kumar, K. A.; Goud, N. R.; Nangia, A., Fluoroquinolone salts with carboxylic acids. *Journal of pharmaceutical sciences* **2011,** *100* (8), 3160-3176.

61. Huang, X.-F.; Zhang, Z.-H.; Zhang, Q.-Q.; Wang, L.-Z.; He, M.-Y.; Chen, Q.; Song, G.-Q.; Wei, L.; Wang, F.; Du, M., Norfloxacin salts with benzenedicarboxylic acids: charge-assisted hydrogen-bonding recognition and solubility regulation. *CrystEngComm* **2013,** *15* (30), 6090-6100.

62. Saifullah, B.; Hussein, M. Z.; Hussein-Al-Ali, S. H.; Arulselvan, P.; Fakurazi, S., Sustained release formulation of an anti-tuberculosis drug based on para-amino salicylic acid-zinc layered hydroxide nanocomposite. *Chemistry Central Journal* **2013,** *7* (1), 72.

63. Li, H.; Wang, K.; Sun, Y.; Lollar, C. T.; Li, J.; Zhou, H.-C., Recent advances in gas storage and separation using metal–organic frameworks. *Materials Today* **2018,** *21* (2), 108-121.

64. Zhao, X.; Wang, Y.; Li, D. S.; Bu, X.; Feng, P., Metal–organic frameworks for separation. *Advanced Materials* **2018,** *30* (37), 1705189.

65. Li, D.; Xu, H.-Q.; Jiao, L.; Jiang, H.-L., Metal-organic frameworks for catalysis: state-of-the-art, challenges, and opportunities. *EnergyChem* **2019**, 100005.

66. Kumar, P.; Deep, A.; Kim, K.-H., Metal organic frameworks for sensing applications. *TrAC Trends in Analytical Chemistry* **2015,** *73*, 39-53.

67. Wang, L.; Zheng, M.; Xie, Z., Nanoscale metal–organic frameworks for drug delivery: a conventional platform with new promise. *Journal of Materials Chemistry B* **2018,** *6* (5), 707-717.

68. Cai, W.; Wang, J.; Chu, C.; Chen, W.; Wu, C.; Liu, G., Metal–Organic Framework-Based Stimuli-Responsive Systems for Drug Delivery. *Advanced Science* **2019,** *6* (1), 1801526.

69. Ibrahim, M.; Sabouni, R.; A Husseini, G., Anti-cancer drug delivery using metal organic frameworks (MOFs). *Current medicinal chemistry* **2017,** *24* (2), 193-214.

70. Furukawa, H.; Cordova, K. E.; O'Keeffe, M.; Yaghi, O. M., The chemistry and applications of metal-organic frameworks. *Science* **2013,** *341* (6149), 1230444.

71. Wu, M. X.; Yang, Y. W., Metal–organic framework (MOF)-based drug/cargo delivery and cancer therapy. *Advanced Materials* **2017,** *29* (23), 1606134.

72. Park, K. S.; Ni, Z.; Côté, A. P.; Choi, J. Y.; Huang, R.; Uribe-Romo, F. J.; Chae, H. K.; O'Keeffe, M.; Yaghi, O. M., Exceptional chemical and thermal stability of zeolitic imidazolate frameworks. *Proceedings of the National Academy of Sciences* **2006,** *103* (27), 10186-10191.

73. Pan, Y.; Liu, Y.; Zeng, G.; Zhao, L.; Lai, Z., Rapid synthesis of zeolitic imidazolate framework-8 (ZIF-8) nanocrystals in an aqueous system. *Chemical Communications* **2011,** *47* (7), 2071-2073.

74. Zheng, H.; Zhang, Y.; Liu, L.; Wan, W.; Guo, P.; Nyström, A. M.; Zou, X., One-pot synthesis of metal–organic frameworks with encapsulated target molecules and their applications for controlled drug delivery. *Journal of the American chemical society* **2016,** *138* (3), 962-968.

75. Kaur, H.; Mohanta, G. C.; Gupta, V.; Kukkar, D.; Tyagi, S., Synthesis and characterization of ZIF-8 nanoparticles for controlled release of 6-mercaptopurine drug. *Journal of Drug Delivery Science and Technology* **2017,** *41*, 106-112.

76. Zhuang, J.; Kuo, C.-H.; Chou, L.-Y.; Liu, D.-Y.; Weerapana, E.; Tsung, C.-K., Optimized metal–organic-framework nanospheres for drug delivery: evaluation of small-molecule encapsulation. *ACS nano* **2014,** *8* (3), 2812-2819.

77. Gomar, M.; Yeganegi, S., Adsorption of 5-fluorouracil, hydroxyurea and mercaptopurine drugs on zeolitic imidazolate frameworks (ZIF-7, ZIF-8 and ZIF-9). *Microporous and Mesoporous Materials* **2017,** *252*, 167-172.

78. Liédana, N.; Galve, A.; Rubio, C. s.; Téllez, C.; Coronas, J., CAF@ ZIF-8: one-step encapsulation of caffeine in MOF. *ACS applied materials & interfaces* **2012,** *4* (9), 5016-5021.

79. Duan, Y.; Ye, F.; Huang, Y.; Qin, Y.; He, C.; Zhao, S., One-pot synthesis of a metal–organic framework-based drug carrier for intelligent glucose-responsive insulin delivery. *Chemical communications* **2018,** *54* (42), 5377-5380.

80. Feng, Y.; Zhong, L.; Bilal, M.; Tan, Z.; Hou, Y.; Jia, S.; Cui, J., Enzymes@ ZIF-8 nanocomposites with protection nanocoating: stability and acid-resistant evaluation. *Polymers* **2019,** *11* (1), 27.

81. Shi, J.; Wang, X.; Zhang, S.; Tang, L.; Jiang, Z., Enzyme-conjugated ZIF-8 particles as efficient and stable Pickering interfacial biocatalysts for biphasic biocatalysis. *Journal of Materials Chemistry B* **2016,** *4* (15), 2654-2661.

82. Lian, X.; Fang, Y.; Joseph, E.; Wang, Q.; Li, J.; Banerjee, S.; Lollar, C.; Wang, X.; Zhou, H.-C., Enzyme–MOF (metal–organic framework) composites. *Chemical Society Reviews* **2017,** *46* (11), 3386-3401.

83. Hou, C.; Wang, Y.; Ding, Q.; Jiang, L.; Li, M.; Zhu, W.; Pan, D.; Zhu, H.; Liu, M., Facile synthesis of enzyme-embedded magnetic metal–organic frameworks as a reusable mimic multi-enzyme system: mimetic peroxidase properties and colorimetric sensor. *Nanoscale* **2015,** *7* (44), 18770-18779.

84. Zhu, Q.; Zhuang, W.; Chen, Y.; Wang, Z.; Villacorta Hernandez, B.; Wu, J.; Yang, P.; Liu, D.; Zhu, C.; Ying, H., Nano-biocatalysts of Cyt c@ ZIF-8/GO composites with high recyclability via a de novo approach. *ACS applied materials & interfaces* **2018,** *10* (18), 16066-16076.

85. Wang, C.; Sudlow, G.; Wang, Z.; Cao, S.; Jiang, Q.; Neiner, A.; Morrissey, J. J.; Kharasch, E. D.; Achilefu, S.; Singamaneni, S., Metal-Organic Framework Encapsulation Preserves the Bioactivity of Protein Therapeutics. *Advanced healthcare materials* **2018,** *7* (22), 1800950.

86. Chu, C.; Su, M.; Zhu, J.; Li, D.; Cheng, H.; Chen, X.; Liu, G., Metal-Organic Framework Nanoparticle-Based Biomineralization: A New Strategy toward Cancer Treatment. *Theranostics* **2019,** *9* (11), 3134.

87. Ran, J.; Wang, C.; Zhang, J.; Wang, W.; Xiao, L.; Jia, S.; Wang, Z.; Wu, W.; Xiao, J.; Wu, X., New insight into polydopamine@ ZIF-8 nanohybrids: A zinc-releasing container for potential anticancer activity. *Polymers* **2018,** *10* (5), 476.

88. Krężel, A.; Maret, W., The biological inorganic chemistry of zinc ions. *Archives of biochemistry and biophysics* **2016,** *611*, 3-19.

89. Costello, L. C.; Franklin, R. B., Decreased zinc in the development and progression of malignancy: an important common relationship and potential for prevention and treatment of carcinomas. *Expert opinion on therapeutic targets* **2017,** *21* (1), 51-66.

90. Costello, L. C.; Franklin, R. B., The clinical relevance of the metabolism of prostate cancer; zinc and tumor suppression: connecting the dots. *Molecular cancer* **2006,** *5* (1), 17.

91. Franklin, R. B.; Milon, B.; Feng, P.; Costello, L. C., Zinc and zinc transporters in normal prostate function and the pathogenesis of prostate cancer. *Frontiers in bioscience: a journal and virtual library* **2005,** *10*, 2230.

92. Franklin, R. B.; Costello, L. C., Zinc as an anti-tumor agent in prostate cancer and in other cancers. *Archives of biochemistry and biophysics* **2007,** *463* (2), 211-217.

93. Costello, L. C.; Franklin, R. B., Cytotoxic/tumor suppressor role of zinc for the treatment of cancer: an enigma and an opportunity. *Expert review of anticancer therapy* **2012,** *12* (1), 121-128.

94. Smith, M. R.; Antonarakis, E. S.; Ryan, C. J.; Berry, W. R.; Shore, N. D.; Liu, G.; Alumkal, J. J.; Higano, C. S.; Maneval, E. C.; Bandekar, R., Phase 2 study of the safety and antitumor activity of apalutamide (ARN-509), a potent androgen receptor antagonist, in the high-risk nonmetastatic castration-resistant prostate cancer cohort. *European urology* **2016,** *70* (6), 963-970.

95. Chi, K. N.; Bjartell, A.; Dearnaley, D.; Saad, F.; Schröder, F. H.; Sternberg, C.; Tombal, B.; Visakorpi, T., Castration-resistant prostate cancer: from new pathophysiology to new treatment targets. *European urology* **2009,** *56* (4), 594-605.

96. Scher, H. I.; Sawyers, C. L., Biology of progressive, castration-resistant prostate cancer: directed therapies targeting the androgen-receptor signaling axis. *Journal of Clinical Oncology* **2005,** *23* (32), 8253-8261.

97. Chen, C. D.; Welsbie, D. S.; Tran, C.; Baek, S. H.; Chen, R.; Vessella, R.; Rosenfeld, M. G.; Sawyers, C. L., Molecular determinants of resistance to antiandrogen therapy. *Nature medicine* **2004,** *10* (1), 33.

98. Clegg, N. J.; Wongvipat, J.; Joseph, J. D.; Tran, C.; Ouk, S.; Dilhas, A.; Chen, Y.; Grillot, K.; Bischoff, E. D.; Cai, L., ARN-509: a novel antiandrogen for prostate cancer treatment. *Cancer research* **2012,** *72* (6), 1494-1503.

99. Koukourakis, M. I.; Kakouratos, C.; Kalamida, D.; Mitrakas, A.; Pouliliou, S.; Xanthopoulou, E.; Papadopoulou, E.; Fasoulaki, V.; Giatromanolaki, A., Comparison of the effect of the antiandrogen apalutamide (ARN-509) versus bicalutamide on the androgen receptor pathway in prostate cancer cell lines. *Anti-cancer drugs* **2018,** *29* (4), 323-333.

APPENDIX A

THE LOADING EFFICIENCY OF APA@ZIF-8

Apalutamide standard calibration curve performed by HPLC is shown below.

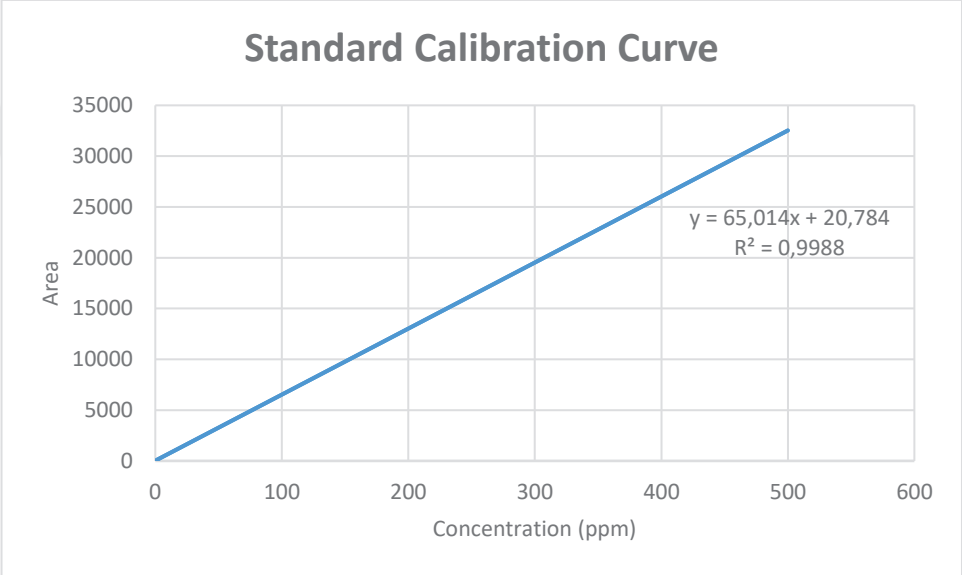

Figure 1. The standard calibration curve of Apalutamide ranging from 1 to 500 ppm

According to the calibration curve shown above, calibration curve equation is:

$$y = 65{,}014x + 20.784$$

Reaction supernatant area = 16349,87

The calculation of supernatant concentration (ppm):

$$16349{,}869 = 65{,}014x + 20.784$$

$$x = 277.05\ ppm$$

Considering 1200 ppm reaction medium:

$$Loading\ efficiency\ (\%) = \frac{1200\ ppm - 277.046\ ppm}{1200\ ppm} \times 100 = 76.91\ \%$$

Considering 6 mg of APA in reaction medium and 76.91 %, the amount of APA encapsulated is expected to be;

$$APA\ amount\ loaded\ at\ APA@ZIF8\ (mg) = \frac{6\ mg\ \times 76.91}{100}$$

$$= 4.62\ \ mg\ APA\ present$$